Development of a microfluidic paper-based device for point-of-care measurement of serum Cystatin C in chronic kidney disease

by

Amir Hossein Abolfathi

A Thesis submitted to the Faculty of Graduate Studies of
The University of Manitoba
In partial fulfilment of the requirements for the degree of

Master of Science

Biomedical Engineering Program
Price Faculty of Engineering
University of Manitoba
Winnipeg, Manitoba, Canada

Publication list

The following is a list of the author's publications during the course of the graduate program. The publication directly incorporated into the thesis or significantly contributed to its development is listed under "Publications included in this thesis". This manuscript has been revised to solely reflect my efforts in the research project. An additional publication completed during the same period but not directly related to the thesis content is listed under "Other publication by the author."

Publications included in this thesis

- D. Tomsa*, Y. Liu*, **A. H. Abolfathi***, X. Ren, A. Stefanson, N. Palmerley, A. A. H. Sokoro, P. Komenda, N. Tangri, R. P. Zahedi, C. Rigatto, and F. Lin, "Integrated microfluidic immunoassays for point-of-care diagnostic measurement of human serum Cystatin C in chronic kidney disease," *manuscript submitted for publication*, Apr. 26, 2025.

* Co-first authors and contributed equally to this study

Other publications by the author

- N. Palmerley, Y. Liu, A. Stefanson, D. Tomsa, **A. H. Abolfathi**, L. Liu, X. Jiang, R. Zahedi, J. Wilkins, R.-C. Su, and F. Lin, "Differential migratory responses of human neutrophils and breast cancer cells to wireless direct current electric field," *in preparation*.

Posters

- **A. H. Abolfathi**, Y. Liu, X. Ren, D. Tomsa, N. Palmerley, A. Stefanson, A. A. H. Sokoro, P. Komenda, N. Tangri, C. Rigatto, and F. Lin, "Microfluidic paper-based analytical device for urine biomarkers analysis in chronic kidney disease, low-cost point-of-care urine biomarker testing," *presented at the Manitoba Materials Conference*, 2024.
- Y. Liu, D. Tomsa, X. Jiang, **A. H. Abolfathi**, N. Palmerley, J. A. Wilkins, R. P. Zahedi, and F. Lin, "Pseudopodia proteome for compositional characterizations of migrating T cells using 3D printed cell protrusion isolation devices," *presented at the μTAS Conference*, 2024.
- N. Palmerley, Y. Liu, A. Stefanson, D. Tomsa, **A. H. Abolfathi**, X. Jiang, R. P. Zahedi, J. A. Wilkins, R. Su, and F. Lin, "Differential migratory responses of cancer cell and immune cell to wireless electrical stimulation," *presented at the μTAS Conference*, 2024.
- **A. H. Abolfathi**, Y. Liu, X. Ren, D. Tomsa, N. Palmerley, A. Stefanson, A. A. H. Sokoro, P. Komenda, N. Tangri, C. Rigatto, and F. Lin, "An integrated microfluidic platform for point-of-care measurements of blood and urine biomarkers in chronic kidney disease," *presented at the Manitoba Materials Conference*, 2025.

Abstract

In clinical practice of chronic kidney disease (CKD), Cystatin C (CYS-C) is recommended as a superior serum biomarker for the estimated glomerular filtration rate (eGFR) compared to the traditional sole creatinine-based eGFR equation, owing to its minimal influence by non-filtration-specific factors such as muscle mass, age, and gender. However, the current CYS-C test is limited to specialized diagnostic labs and no point-of-care (POC) tools are clinically available. To address this gap, we leveraged the enabling power of microfluidic devices for POC tests of CYS-C. Among the various types of microfluidic devices, paper-based dry chips have been widely used for disease biomarker measurements with their respective advantages and limitations. Therefore, in this study, we developed a paper-based microfluidic lateral flow immunoassay chip with a unique channel design and a novel electric field-assisted antibody loading protocol for quantitative CYS-C tests. We demonstrated that paper chips meet the clinical requirements of the serum CYS-C detection range and limit. Importantly, this microfluidic chip is packaged into a special housing cartridge integrated with a custom-developed portable reader. The reader is wirelessly controlled by a smartphone app as a POC test prototype. In validation studies using serum samples from CKD patients across different disease stages, the proposed chip tests showed a similar agreement level with the traditional well plate-based immunoturbidity assay test results. As an integrated POC test system, the microfluidic CYS-C paper chip test showed high accuracy to determine the eGFR range based on several clinically relevant grouping criteria. Collectively, this integrated microfluidic assay offers practical solutions for decentralized POC diagnostic tests of CKD with competitive advantages over existing methods.

Acknowledgements

I would like to express my sincere gratitude to Prof. Francis Lin for his invaluable support and guidance throughout this program. Under his supervision, I was fortunate to explore diverse scientific fields beyond what I had envisioned possible within a two-year timeframe. His insightful and constructive feedback on my publications, including manuscripts and poster presentations, consistently inspired and motivated me. Particularly memorable was our collaborative effort on a poster, where his dedication was evident as we exchanged communications well into midnight. Prof. Lin's distinctive perspectives and careful attention to various aspects of my project have significantly enriched my academic experience and contributed to my academic success.

I am deeply grateful to my advisory committee members, Dr. AbdulRazaq A. H. Sokoro and Dr. Song Liu, for their valuable feedback and thoughtful evaluations throughout this journey. Having experts from different scientific backgrounds on my committee has been an incredible privilege, offering me diverse perspectives that have enriched my research. I am deeply grateful for the time, attention, and commitment you dedicated to reviewing my work and evaluating my academic progress.

I would like to extend my sincere gratitude to the Price Faculty of Engineering and the program coordinators of the Biomedical Engineering program for making an environment for students from different backgrounds to flourish. I would also like to appreciate the Department of Physics and Astronomy for providing a welcoming space for graduate students.

To my lab mates, Dumitru Tomsa, Nicholas Palmerley, Dr. Yang Liu, and Dr. Amanda Stefanson, I appreciate your assistance in different stages of my study. I am truly

thankful for having the chance to work in an environment where everyone is willing to open-handedly share their knowledge and provide assistance at any time. Many thanks to Dr. Yang Liu, the person who dedicated her time and commitment to my training. Without her commitment, I would have never been able to proceed significantly in my studies.

I gratefully acknowledge Dr. Elham Salimi's important role in building the basis for my microfluidics knowledge. Having a clear view and strong background knowledge strongly supported my studies. Thanks to the Seven Oaks General Hospital and Victoria General Hospital for providing real samples for evaluating my improvements in real testing. Many thanks to AssureCKD, Inc. for their financial support through a sponsored research agreement in this project. I would like to deeply express my gratitude for their sponsorship as my scientific project would not progress without their support.

Finally, I am forever grateful for the unlimited support from my parents and my partner. Academic life is known to be mentally intensive, and emotional support is necessary to keep up the good work. I hope passing this milestone satisfies my parents' expectations of their forever-grateful son. This journey would not have been possible without the constant support of my partner. Thank you for always being there for me, regardless of your unbearable workload.

Table of contents

List of tables

List of figures

Abbreviations

3D	Three-Dimensional
AKI	Acute Kidney Injury
AuNP	Gold Nanoparticle
B-A	Bland–Altman
BLE	Bluetooth Low Energy
BSA	Bovine Serum Albumin
C	Control area (on lateral flow tests)
CKD	Chronic Kidney Disease
CKD-EPI	Chronic Kidney Disease Epidemiology Collaboration
CKD-MBD	Chronic Kidney Disease–Mineral and Bone Disorder
COVID-19	Coronavirus Disease 2019
CRE	Creatinine
CRP	C-Reactive Protein
CYS-C	Cystatin C
DC	Direct Current
EF	Electric Field
ELISA	Enzyme-Linked Immunosorbent Assay

GFR	Glomerular Filtration Rate
HSA	Human Serum Albumin
IEP	Immunoelectrophoresis
IVD	In Vitro Diagnostics
IgG	Immunoglobulin G
LED	Light Emitting Diode
LFIA	Lateral Flow Immunoassay
LOD	Limit of Detection
MP	Megapixel
NC	Nitrocellulose
NPV	Negative Predictive Value
PBS	Phosphate-Buffered Saline
PDMS	Polydimethylsiloxane
PC	Personal Computer
PLA	Polylactic Acid
PPV	Positive Predictive Value
POC	Point of Care
POCT	Point-of-Care Testing

REASSURED	Real-time connectivity, Ease of specimen collection, Affordable, Sensitive, Specific, User-friendly, Rapid and robust, Equipment-free, and Deliverable to end-users
RGB	Red, Green, Blue
T	Test area (on lateral flow tests)
US	United States
WHO	World Health Organization
eGFR	Estimated Glomerular Filtration Rate
eGFRcr	Estimated GFR using Creatinine
uACR	Urine Albumin-to-Creatinine Ratio

Permission of using published materials

- Figure 1.1 is redesigned from "niddk.nih.gov/health-information/kidney-disease/chronic-kidney-disease-ckd/tests-diagnosis/albuminuria-albumin-urine". The contents from NIDDK are copyright-free and permission request is not needed.
- Figure 1.2 is from "Lekskulchai, V. (2022). Use of Estimated Glomerular Filtration Rate and Urine Albumin-to-Creatinine Ratio Based on KDIGO 2012 Guideline in a Thai Community Hospital: Prevalence of Chronic Kidney Disease and its Risk Factors. Medical Science Monitor Basic Research, 28, e938176.". The figure is licensed under CC BY-NC-ND 4.0, thus non-commercial distribution without any derivation is allowed and permission request is not needed.
- Figure 1.3 is the schematic illustration of a lateral flow immunoassay (LFIA) device. It is created and designed by the author based on general LFIA principles.
- Figure 1.4 is created and designed by the author based on general LFIA principles and paper-based microfluidics concept.
- Figures 2.1, 2.2, 2.3, 2.4, 2.5, 2.6, and 2.7 are from my paper "Tomsa, D., Liu, Y., **Abolfathi, A. H.**, Ren, X., Stefanson, A., Palmerley, N., Sokoro, A. A. H., Komenda, P., Tangri, N., Zahedi, R. P., Rigatto, C., & Lin, F. (2025, April 26). Integrated microfluidic immunoassays for point-of-care diagnostic measurement of human serum Cystatin C in chronic kidney disease [Manuscript submitted for publication]."

Chapter one: An overview of chronic kidney disease biomarker testing, literature review

1.1. Chronic kidney disease, pathology, and complications

Chronic Kidney Disease (CKD) is a progressive condition characterized by irreversible damage to the kidney's structure and function. This damage primarily affects functions as a selective barrier [1], [2]. Common risk factors include diabetes mellitus, hypertension, and obesity [3]. CKD affects approximately 13% of the global population and is associated with systemic complications involving the cardiovascular and musculoskeletal systems, underscoring the critical need for early detection. The crosstalk between kidney dysfunction and other organ systems can progress to cardiorenal syndrome and CKD–mineral and bone disorder (CKD–MBD). These complications highlight the systemic nature of CKD and reinforce the importance of timely diagnosis in reducing disease burden and mortality [4].

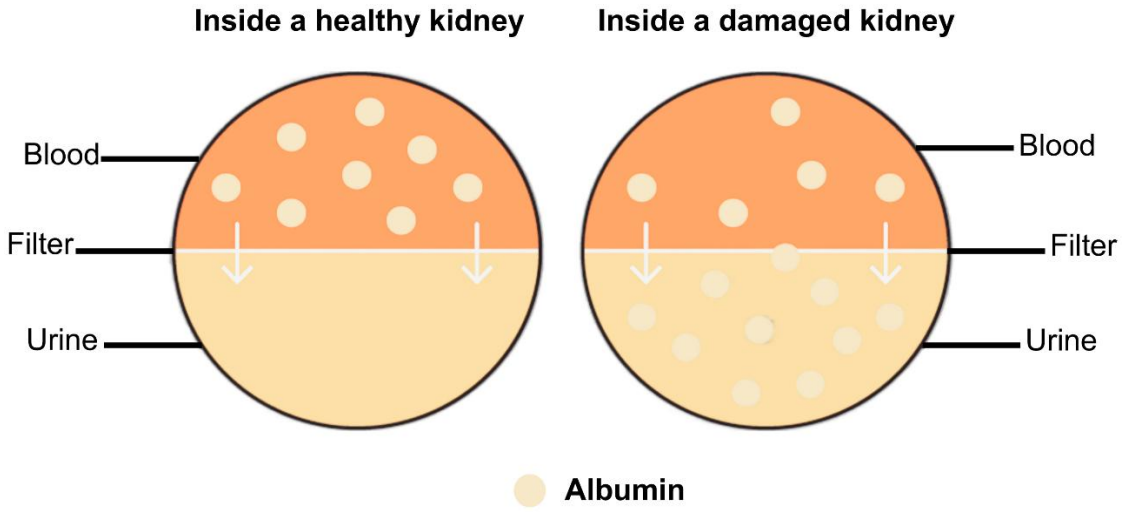

Figure 1.1. The impaired kidney filtration is illustrated through the urinary release of a common biomarker, the albumin protein (Adapted from NIDDK).

The pathophysiology of CKD is complex and continues to evolve, with several areas still under active investigation. These include metabolic and neuroendocrine alterations associated with disease progression [4], as well as the identification of biomarkers with stronger predictive value. Currently, most clinical biomarkers for CKD focus on glomerular function, particularly the glomerular filtration rate (GFR). Among these, serum creatinine remains the most widely used marker. Creatinine is a metabolic byproduct found in bodily fluids and is normally excreted by the kidneys. As CKD progresses, structural damage to the glomeruli impairs their filtration capacity, leading to elevated creatinine levels in the blood and altered concentrations in urine. These changes form the basis for calculating the estimated glomerular filtration rate (eGFR), a critical metric used in CKD staging and risk assessment.

A key limitation of relying solely on serum creatinine for CKD staging is that changes in creatinine levels do not always reflect early glomerular damage. This is partly due to the redundancy and reserve capacity of the kidneys, individuals with a high number of functional nephrons may maintain normal filtration rates despite underlying injury. In such cases, subclinical kidney damage may go undetected if creatinine is used as the only marker. Moreover, the creatinine content is related to a number of non-renal factors that must be corrected when used for eGFR calculation. For instance, people with higher muscle mass have higher urine creatinine levels, the same as people suffering from muscle atrophy. Race, sex, and age are other factors that have been identified to contribute to creatinine levels of the body [2].

The unreliability of Creatinine (CRE) levels for eGFR has led to revisions for eGFR calculation formulas in order to improve the prediction levels. There are currently 3

different eGFR equations: CKD-EPI creatinine equation (2021), CKD-EPI creatinine-cystatin equation (2021), and CKD-EPI Cystatin C equation (2012). These calculations use parameters like CKD serum biomarker contents, age, gender, and body surface area (height and weight), and based on the eGFR value, cases with filtration rates of less than 60 mL/min/1.73m^2 are considered as CKD patients [5].

1.2. Reliable screening tools for CKD

For a more relevant and precise prediction of CKD progression in the body, it is necessary to consider additional biomarkers. CYS-C, albumin, and the urine albumin-to-creatinine ratio (uACR) are important indicators used by medical professionals to stage CKD cases. Serum CYS-C is included in two of the most commonly used eGFR equations, and pairing uACR with eGFR improves CKD staging accuracy.

Urine Albumin, a component of uACR, is known to be a vital tool for kidney damage assessments. A healthy kidney filters 3.3 grams of Albumin per day from the blood, and it is expected to recycle 3.2 grams [6]. This process is performed through the tubular reabsorption; damages to tubular bodies and saturation of reabsorption causes the uprise of albumin in CKD cases. This also suggests that glomerular filtration rate could be independent of excess albumin excretion in urine. In other words, a person with normal eGFR could still be in risk of kidney damage; hence the importance of including albumin in the diagnosis procedure.

Urine albumin-to-creatinine ratio is classified into 3 levels of kidney damage; A1, <30 mg/g; A2, 30 to 300 mg/g; and A3, >300 mg/g. The first level, A1, is considered a low risk of developing kidney damage with the condition of normal eGFR, and higher risks depend on assessments of both uACR and eGFR using the chart below (**Figure 1.2**).

eGFR categories	eGFR	Categories of persistent albuminuria		
		A1	A2	A3
		UACR <3	UACR=3-30	UACR >30
G1	≥90	Low risk	Moderate risk	High risk
G2	60-89	Low risk	Moderate risk	High risk
G3a	45-59	Moderate risk	High risk	Very high risk
G3b	30-44	High risk	Very high risk	Very high risk
G4	15-29	Very high risk	Very high risk	Very high risk
G5	<15	Very high risk	Very high risk	Very high risk

eGFR in mL/min/1.73 m^2 and UACR in mg/mmol creatinine. eGFR – estimated glomerular filtration rate; UACR – urine albumin-creatinine ratio.

Figure 1.2. CKD risk assessment chart. Combining urinary albumin-to-creatinine ratio (uACR) and estimated glomerular filtration rate provides a risk assessment tool for clinicians [7].

Urinary albumin excretion is commonly assessed using a 24-hour urine collection, which requires patients to collect all voided urine over a full day. However, this method is prone to several pre-analytical errors, including incomplete collection, sample contamination, and loss, particularly in elderly patients and pediatric settings. As an alternative, first-morning urine samples are often recommended due to their improved stability, reduced diurnal variation, and lower susceptibility to user error. Nevertheless, urine albumin remains a biomarker with significant variability, influenced by collection methods and the inherent limitations of protein quantification techniques [8].

1.3. Cystatin C, a reliable CKD screening biomarker

In recent decades, CYS-C has emerged as a valuable biomarker for kidney function assessment, offering several advantages over traditional markers. CYS-C is a low-molecular-weight cysteine protease inhibitor produced at a relatively constant rate by all nucleated cells. It is freely filtered by the glomeruli and subsequently reabsorbed and metabolized by proximal tubular cells, making it less susceptible to non-renal influences such as muscle mass, age, sex, and race. Due to its improved stability and predictive value, CYS-C has been incorporated into estimated glomerular filtration rate (eGFR) equations, including the CKD-EPI Cystatin C equation (2012) and the CKD-EPI Creatinine-Cystatin C equation (2021). These models offer improved accuracy and, in newer versions, exclude race-based adjustments, addressing concerns around bias and variability in kidney function estimation. As clinical guidelines increasingly recognize CYS-C as a preferred biomarker for CKD screening in adults, the demand for reliable, cost-effective, and accurate assays has grown, motivating the development of improved analytical platforms for serum-based testing [9].

1.4. Common clinical practice in Cystatin C quantification

Currently, the clinical practice for serum CYS-C quantification relies on immunoturbidimetric and immunonephelometric methods. These methods are based on the bonding between the analyte (CYS-C) and antibodies. Samples are added to antibody-labeled polymers, creating insoluble complexes that scatter light beams. The more reacted analytes, the more scatter is recorded by the analyzer, the nephelometer. Although there are arguments about the accuracy of measurements by these methods, ease of automation has made them a preferred practice. Required reagents are developed and available by a number of companies and the assay procedure is fairly straightforward in terms of laboratory practice [9].

Clinical laboratory methods provide the accuracy and precision necessary for diagnostic decision-making; however, they are often associated with high costs, complex instrumentation, and the need for trained personnel. Such tests are typically conducted in certified laboratories, limiting accessibility for frequent monitoring. Individuals with type 1 and type 2 diabetes mellitus, who are at elevated risk for developing CKD, require regular monitoring of kidney biomarkers. For these patients, especially the elderly or those with comorbid conditions, frequent travel to clinical facilities can be troublesome, both physically and financially. To address these challenges, the concept of point-of-care testing (POCT) has emerged as a practical alternative. POCT platforms are typically compact, user-friendly, and designed for deployment in decentralized settings such as homes, clinics, and mobile units. Recognizing this growing need, various international standards and guidelines have been developed to assist researchers and manufacturers in designing effective POCT tools for disease screening and biomarker detection.

1.5. Point-of-care testing, a solution for the growing need

The increasing global prevalence of CKD and the financial burden associated with conventional laboratory-based diagnostics underscore the need for developing POCT solutions. POCT, also referred to as bedside testing, enables rapid, on-site analysis of clinical samples, reducing the dependency on centralized laboratories and facilitating timely clinical decision-making [10]. To guide the development of effective and accessible POCT tools, the World Health Organization (WHO) introduced the REASSURED criteria. This framework emphasizes key attributes that such platforms should meet: Real-time connectivity, Ease of specimen collection, Affordable, Sensitive, Specific, User-friendly, Rapid and robust, Equipment-free, and Deliverable to end users. By adhering to these principles, researchers and developers can align diagnostic innovations with global public health needs, particularly in resource-limited settings [11].

1.6. Great examples of POCT

Widely used REASSURED-compliant diagnostic tools include dipsticks and lateral flow immunoassays (LFIAs), such as pregnancy tests and certain COVID-19 kits. Among them, urinary albumin-to-creatinine ratio (uACR) dipsticks are commercially available for semi-quantitative screening of CKD biomarkers. Although these assays offer ease of use and rapid results, they lack the analytical precision required for detailed risk assessment and clinical decision-making. The LFIA format has played a significant role in point-of-care diagnostics, offering advantages such as low cost, portability, and minimal user training. There are two primary LFIA formats: noncompetitive (sandwich) and competitive assays. The noncompetitive format is well-suited for detecting high-molecular-weight analytes such as proteins and antigens, making it the preferred approach in this study. In

contrast, the competitive format is typically used for low-molecular-weight compounds like hormones or small drugs. Traditionally, LFIAs have been employed for qualitative measurements, as seen in pregnancy and COVID-19 tests, where a colorimetric signal indicates a positive result. However, recent advancements have focused on quantitative adaptations of this format, expanding its utility in clinical diagnostics [12].

1.7. Traditional lateral flow immunoassays; a rapid qualitative testing

A typical lateral flow immunoassay (LFIA) device (**Figure 1.3**) consists of a strip of nitrocellulose (NC) membrane with pore sizes up to 12 μm, mounted on a plastic backing for support. At one end of the strip, a sample pad is positioned, which contains antibody-conjugated detection particles, commonly gold nanoparticles or latex beads. When the sample is applied, target analytes bind to the antibodies on the surface of these particles, forming an analyte-antibody complex. The mixture migrates along the strip via capillary action, passing through the test and control zones. In the test zone, immobilized capture antibodies specific to the analyte bind the analyte-particle complex, resulting in a visible signal (usually a colored line). The control zone contains secondary antibodies that recognize and bind to the detection antibody, confirming proper fluid migration and reagent integrity [12]. At the distal end, an absorbent pad is placed to maintain the capillary flow by drawing the liquid across the membrane. To reduce non-specific binding, the membrane is treated with blocking buffers such as bovine serum albumin (BSA) or casein. Additionally, surfactants like Tween 20 are applied to improve flow dynamics and ensure consistent sample migration.

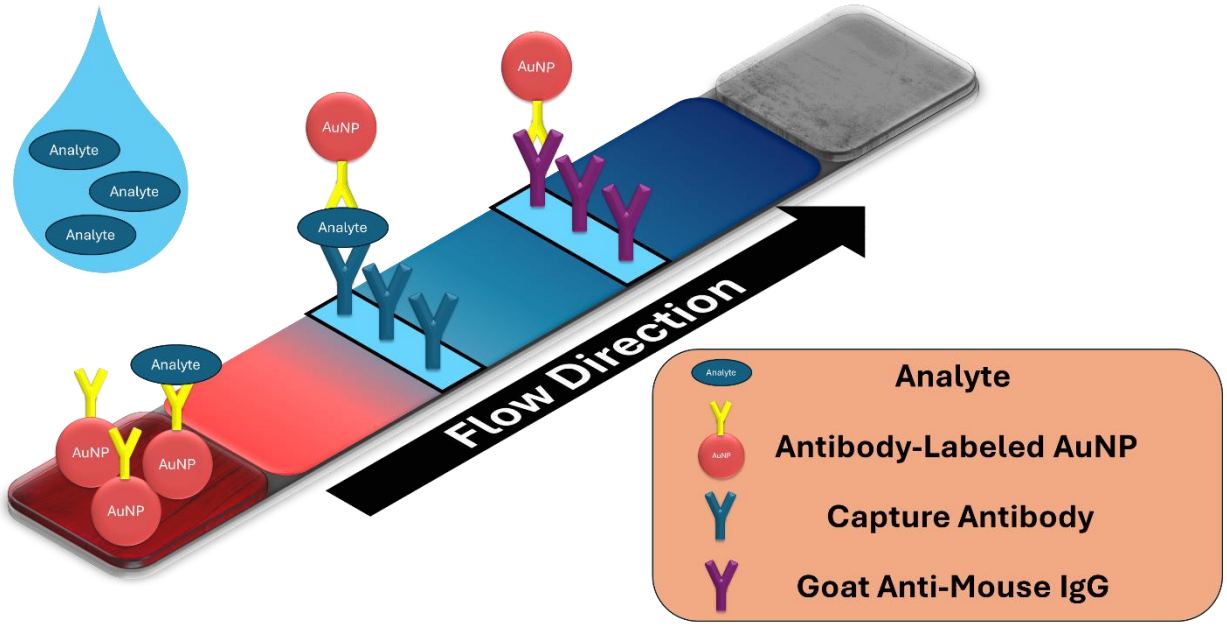

Figure 1.3. The traditional concept of lateral flow immunoassay is presented. The sample containing the analyte is added to the conjugate pad, the place where it reacts with the antibody-labeled AuNPs. The sample mixture is led through wicking to antibody lines.

1.8. Paper-based microfluidic LFIA

Paper-based microfluidics is an analytical platform that enables the controlled manipulation of microliter-scale liquid volumes within porous substrates, most commonly cellulose or nitrocellulose membranes. These substrates support capillary-driven flow, eliminating the need for external pumps and power sources, an essential advantage for point-of-care diagnostics, particularly in resource-limited settings [13]. Paper offers several favorable properties: it is low-cost, lightweight, biodegradable, disposable, and readily modifiable, making it an ideal material for scalable diagnostic device fabrication. Fluid flow is confined and directed through hydrophilic pathways bounded by hydrophobic barriers, which can be created using various patterning techniques. Common fabrication methods include wax printing, screen printing, lamination, plasma treatment, and layer-by-layer assembly. These techniques allow for rapid prototyping of customized channel geometries to control flow rates, reaction times, and reagent distribution [14]. A key advantage of paper-based microfluidic devices is the ease of design iteration and low production cost, particularly when compared to polymer-based microfluidic systems such as PDMS, which often require cleanroom-based lithographic techniques and specialized equipment. As a result, paper-based platforms provide a versatile and accessible alternative for diagnostic assay development.

In this work, we adapt the principles of lateral flow immunoassay (mentioned in the previous section) to a paper-based microfluidic format for the quantitative detection of CYS-C in serum samples (**Figure 1.4**). The test (T) and control (C) zones are positioned along these channels, where immobilized antibodies capture functionalized gold nanoparticles, producing a colorimetric signal that correlates with analyte concentration.

The assay fabrication process begins with pattern printing optimized to focus fluid flow toward the test zone, followed by standard treatment procedures to prepare the device for testing. This integration of LFIA principles with paper microfluidics offers significant advantages, including improved signal control, scalability, and cost-efficiency, aligning well with the requirements of POC diagnostic applications.

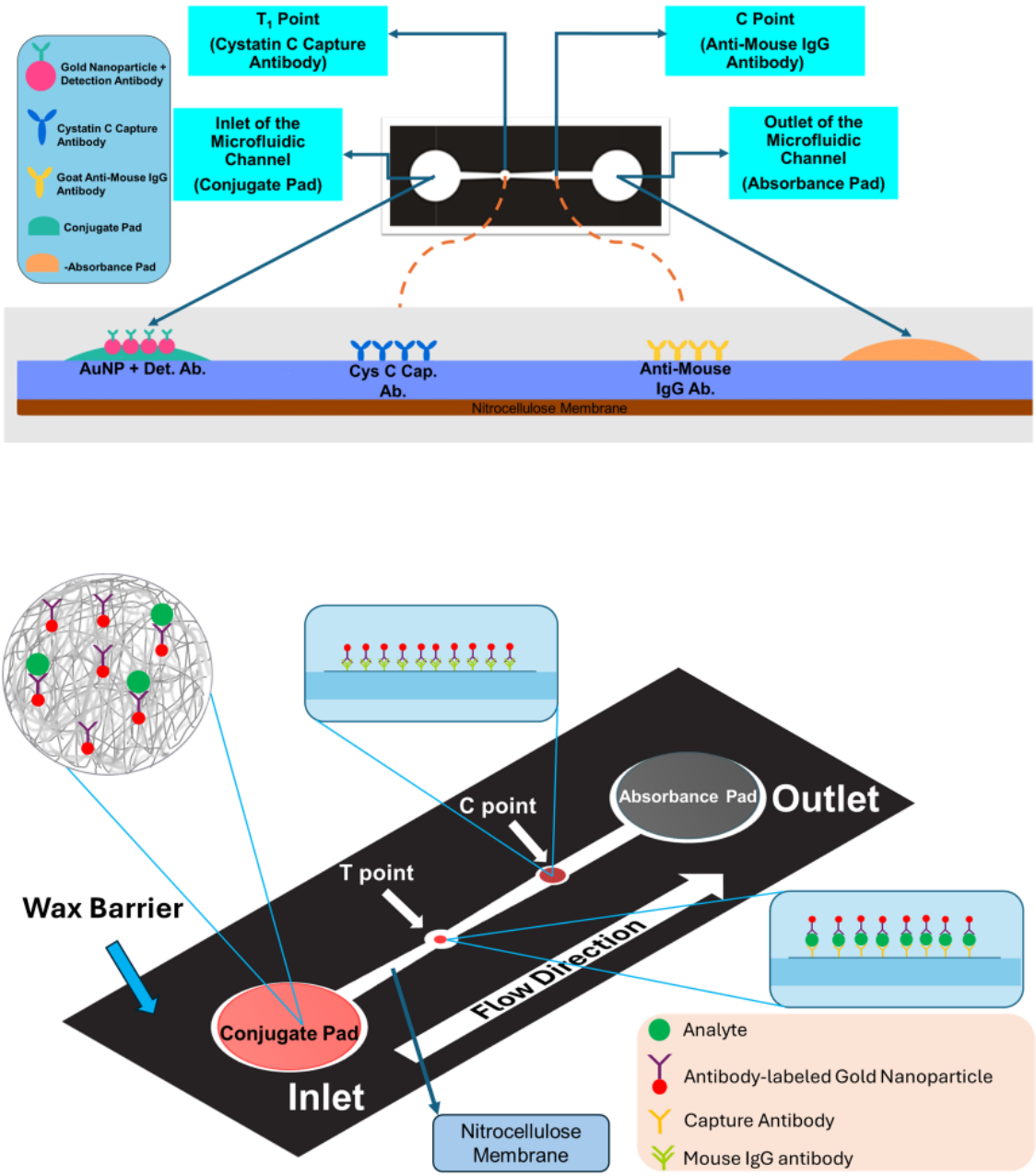

Figure 1.4. The design of the LFIA paper chip is presented in side view(top) and perspective view (bottom). This design is adapted from the lateral flow immunoassay concept and consists of miniaturized essential elements of this engineering.

In this series of studies, we have conducted a comprehensive analysis of paper microfluidic LFIA for CYS-C. Serum CYS-C is among the frequently tested CKD biomarkers, involving a high financial burden on governments and healthcare authorities. In addition, individuals experience a variety of difficulties and restrictions when they are referred to clinical labs for urine and blood tests. Ranging from sample collection, proprietary services and availability in remote areas to technical problems with the testing protocols, we aimed to design biomarker testing with elevated precision and accuracy, along with ease of use for all types of users.

1.9. Thesis layout and chapter summary

Investigating paper microfluidics and its adaptability for LFIA, studying the CKD biomarker testing, and developing POC screening device are the main objectives of the study. As a result, this thesis is structured to present an introduction to CKD biomarker testing, a scientific paper on CYS-C testing using paper-based microfluidics, and a conclusion of the study. The physiology, pathology and testing methods in chronic kidney disease were presented in **Chapter 1**. In the following chapter (**Chapter 2**), the main study is presented in the form of a scientific paper, based on the submission criteria of the ACS Sensors journal. Finally, it is transitioned into a conclusion chapter (**Chapter 3**) outlining the conclusion and expected future directions of the project. The overall layout aims to provide a comprehensive report regarding CKD biomarker testing, focusing on paper microfluidics and the point-of-care aspect of this project.

Chapter Two: Development of a low-cost clinically acceptable microfluidic paper-based testing platform for Cystatin C in chronic kidney disease

This chapter is based on the following publication which is under review:

- D. Tomsa[*], Y. Liu[*], **A. H. Abolfathi[*]**, X. Ren, A. Stefanson, N. Palmerley, A. A. H. Sokoro, P. Komenda, N. Tangri, R. P. Zahedi, C. Rigatto, and F. Lin, "Integrated microfluidic immunoassays for point-of-care diagnostic measurement of human serum Cystatin C in chronic kidney disease," manuscript submitted for publication, Apr. 26, 2025.

[*] Co-first authors and contributed equally to this study

Contribution statement

In this project, two low-cost microfluidic platforms were developed for the quantitative detection of CYS-C, a clinically preferred biomarker for chronic kidney disease (CKD). These platforms include an immunoturbidimetric PDMS-based microfluidic chip and a paper-based lateral flow immunoassay (LFIA).

My contributions focused on the development and validation of the paper-based LFIA platform. I adapted LFIA principles into a microfluidic paper-based format and incorporated an electric-field-assisted antibody alignment strategy to enhance detection sensitivity and precision. In addition, I conducted a comprehensive literature review on paper-based microfluidic diagnostic methods, carried out standard and real-sample testing, and performed data collection and preliminary analysis. I was also responsible for interpreting the experimental results and drafting and revising the thesis sections related to this platform.

2.1. Introduction

Chronic kidney disease (CKD) is defined as the gradual loss of kidney function, including the ability to filter waste, regulate fluid and electrolyte balance, and manage key metabolic processes. Early diagnosis is essential due to the critical role the kidneys play in maintaining health [15]. Globally, kidney disease affects an estimated 860.8 million people. Of these, 843.6 million have CKD (Stages 1–5), while 3.9 million require renal replacement therapy [16], [17]. CKD is not only a global health crisis but also a significant risk factor for kidney failure, cardiovascular disease, and mortality. Although effective treatments exist to slow disease progression, treatment success depends on early detection of CKD, before symptoms or signs of kidney disease appear [18].

Common risk factors for CKD include diabetes, hypertension, heart disease, obesity, and a history of acute kidney injury (AKI) or familial kidney disease [19]. CKD fulfills all the World Health Organization's criteria for a screenable disease: it is common, detectable, and treatable. Despite this, it remains severely underdiagnosed [15], [20], [21]. The high global burden of CKD underscores the lack of widely accessible, reliable tools for early diagnosis. Point-of-care (POC) testing presents a valuable opportunity to support early diagnosis and management, especially in underserved or resource-limited settings [22], [23], [24].

CKD diagnosis typically involves estimating glomerular filtration rate (eGFR), often calculated from serum creatinine. While serum creatinine is widely used, it is influenced by factors such as age, sex, race, muscle mass, and nutrition, limiting its accuracy [25], [26]. In contrast, serum Cystatin C (CYS-C) offers a more reliable biomarker for eGFR estimation. Produced by all nucleated cells, CYS-C levels are stable

and less affected by non-renal factors [27], [28], [29], [30]. Notably, CYS-C has been shown to predict long-term mortality better than creatinine in critically ill patients [31]. Beyond nephrology, CYS-C has been implicated in cardiovascular disease progression and neurodegenerative disorders such as Alzheimer's disease [32], [33], [34], [35], [36].

Despite its clinical value, CYS-C testing remains largely restricted to laboratory settings due to the complexity, cost, and infrastructure required for current methods. Techniques such as ELISA, radioimmunoassays, immunoturbidimetry, fluorescence-based assays, and mass spectrometry are accurate but demand skilled personnel, expensive reagents, and time-intensive workflows [37], [38], [39]. These limitations hinder the widespread adoption of CYS-C testing, especially in primary care or low-resource environments.

To address this gap, a true POC test for CYS-C must balance simplicity, cost-effectiveness, speed, and analytical accuracy. Microfluidic technologies offer a promising foundation for such solutions. By miniaturizing lab processes onto portable chips, microfluidic POC devices can deliver rapid, user-friendly, and reliable diagnostics [23], [40], [41]. Most existing CYS-C microfluidic devices rely on electrochemical sensing, using complex electrode materials—such as ZIF-8-Cu1−xNix(OH)2@Cu [42], graphene composites [43], and MOF-based nanomaterials [44] to enhance performance. While sensitive, these designs are often prohibitively difficult to mass-produce. Turbidimetric and nephelometric detection strategies are more suited to scalable and low-cost implementation but remain underexplored in this context. A continuous-flow microfluidic turbidity sensor was previously developed for non-diagnostic use [45], and a latex immunoagglutination assay for vasculitis marker detection inspired our current direction [46].

In this study, we present a microfluidic paper-based approach for POC quantification of serum CYS-C. This approach involves a paper-based microfluidic lateral flow sandwich immunoassay, a format widely used in diagnostics for infectious diseases and tumor markers [40], [47], [48], [49]. Our device is built on this foundation, introducing innovations to enable quantitative CYS-C detection in a cost-effective, accessible format.

2.2. Materials and Methods

The CYSTATIN-C: ITA Reagent Kit was ordered from Toronto BioScience. Adobe Illustrator was used for designing the paper chip, and the design was printed on Hi-Flow™ Plus Membrane 90 from MilliporeSigma (Burlington, MA, USA) with the ColorQube 8570 solid ink printer. Glass fiber (MilliporeSigma, Cat. # GFDX203000, St. Louis, MO, USA) and cotton absorbent pads (MilliporeSigma, Cat. # CFSP223000, St. Louis, MO, USA) were used for performing the test. Cystatin C detection antibody (HyTest, Cat. No. Cyst28) was conjugated with gold nanoparticles according to the manufacturer's protocol of the Gold Conjugation Kit (Abcam, Cat. No. ab188215). The Cystatin C capture antibody (HyTest, Cat. No. Cyst24cc) was diluted to a working concentration of 1 mg/mL with PBS before loading onto the chip. The human Cystatin C standards were provided by CYSTATIN-C: ITA Reagent Kit. Goat anti-mouse IgG (H+L) antibody was purchased from ThermoFisher Scientific (Cat. No. 31160, 2.32 mg/mL). The USB Microscope AD4113T Premier Series used for paper chip signal acquisition was purchased from Dino-Lite.

2.2.1. Microfluidic Cystatin C paper chip design

The CYS-C paper chip pattern was designed with Adobe Illustrator CC 2017 (**Figure 2.1A**) by including a conjugation pad in the shape of a 7 mm diameter circle; an

absorbance pad in the shape of a 7 mm diameter circle; the absorbent pad serves as the waste reservoir, as well as an additional driving force for capillary flow. The flow channel printed on a nitrocellulose membrane using solid ink connects the conjugation pad and the absorbance pad. It has a channel length of 18.3 mm and includes one detection (T) point and one control (C) point (**Figure 2.1A**). The T and C points are 1.5 mm diameter circles for the immunoassay reaction on the chip. The geometry of the flow channel connecting the conjugation pad to the T point, the T point to the C point, and the C point to the absorbance pad were differently designed to optimize the immunoassay reaction at the T point and C point. Specifically, the channel between the conjugation pad and the T point starts with a broader opening and gradually narrows toward the T point so that the flow reduces at the T point, allowing for increased time of immuno-binding and reaction. Once passing the T point, the channel width gradually increases toward to the C point, accelerating the flow to speed up the assay and reduce the background. Finally, the channel connecting the C point and the absorbance pad was designed with high channel width and short length to more efficiently release the flow to the absorbance pad for waste collection (**Figure 2.1A**).

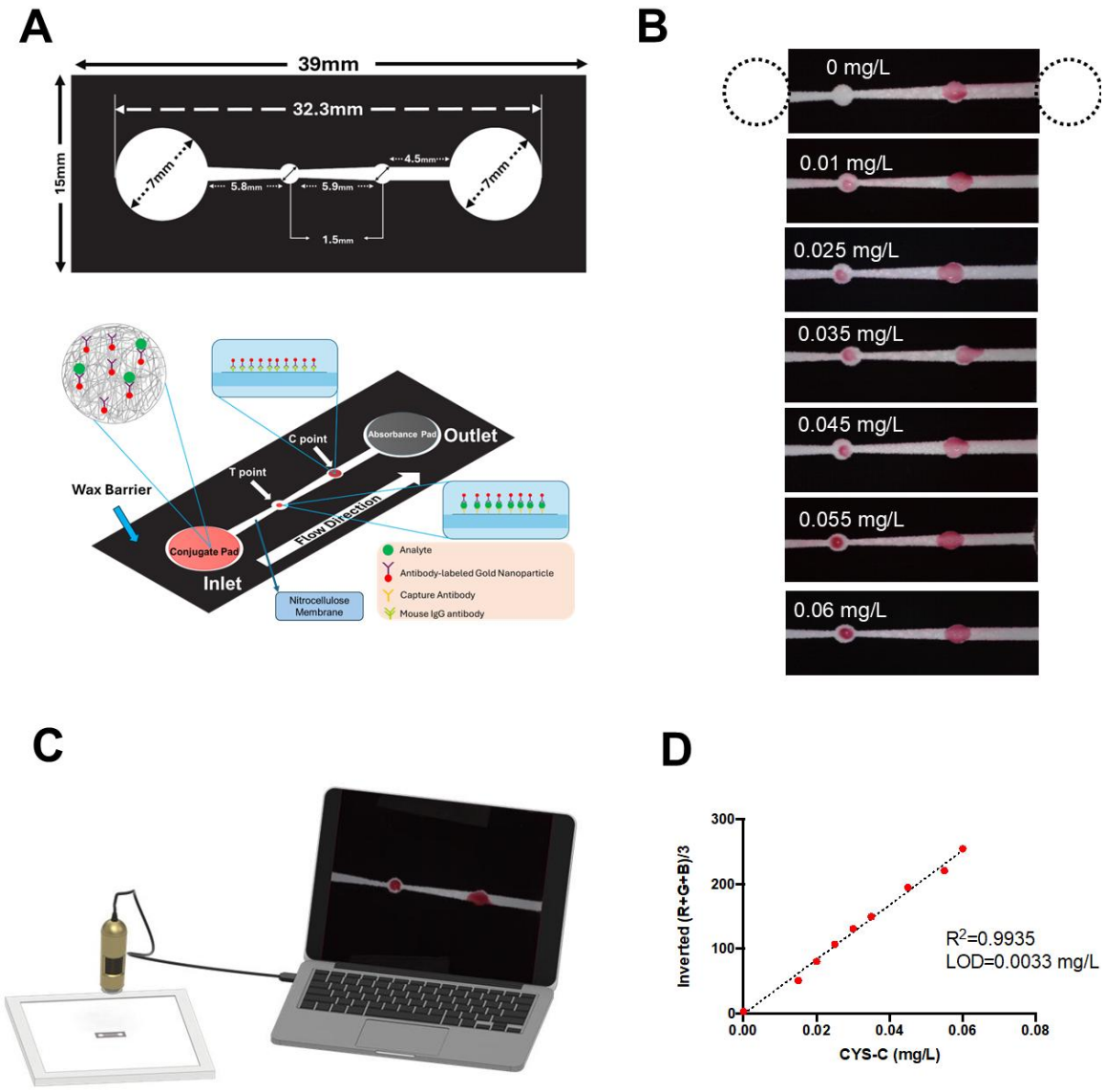

Figure 2.1. Illustration of the paper-based microfluidic CYS-C immunoassay chip and its technical performance. A. The CYS-C immunoassay paper chip design (top) and schematic of the paper chip immunoassay's working mechanism (bottom); **B.** Representative images of the CYS-C paper chip showing the increased color signal intensity at the T point (left) with the increasing CYS-C standard concentrations ranging from 0-0.06 mg/L, and the consistent color signal intensity at the C point (right); The flow direction is from left to right and dotted line circles indicate the conjugation and absorbance

pads; **C.** The color signal from the CYS-C paper chip was imaged by a USB microscope platform with the backlight illumination, and analyzed using an external PC; **D.** The calibration curve of the CYS-C paper chip test based on the inverted (R+G+B)/3 of the color signal at the T point against the CYS-C standard concentrations is shown.

2.2.2. Microfluidic Cystatin C paper chip preparation

The CYS-C paper chips are prepared by printing wax on Hi-Flow™ Plus 90 2 mil backed membrane having a capillary flow rate of 90 seconds / 4 cm to form the flow channels. The wax defines hydrophobic barriers or a hydrophobic boundary region, resulting in microfluidic channels on the hydrophilic paper when the wax is melted at 125°C for 30 seconds by bringing the reverse side of the membrane (the side of the plastic backing) into contact with the heated surface of a hotplate. After the chip pattern has been heated, it cools down to room temperature, resulting in a paper chip that includes a pattern having hydrophobic boundaries (**Figure 2.1A**). CYS-C capture antibody and goat anti-mouse IgG (H+L) control antibody are loaded on the test point and control point (T and C) individually under the effect of an electric field to orient and align antibodies for improved test consistency as detailed in **Figure 2.5**. Using this method, 0.05 μL of each antibody is loaded on the test point and control point and is dried at room temperature for 1 hour. Non-specific binding by the nitrocellulose in the channels is reduced by treating the membrane with a blocking agent, which is typically 0.4 wt% BSA in PBS, and dried at room temperature for around 1 hour before the next step. After the blocking step, the chip is rinsed with 0.1 wt% Tween 20 in PBS and dried at room temperature for approximately 30 minutes. Treatment with surfactant modulates membrane properties upon BSA blocking and thus helps achieve the desirable flow rate. The conjugation pad and absorbance pad were cut into circular shapes with a diameter of 7 mm. The conjugate pad was first treated with 0.4 wt% BSA in PBS and allowed to dry at room temperature. It was then treated with 20 μL of a 0.1 wt% Tween 20 solution followed by 2 μL of AuNP solution, and subsequently dried at room temperature prior to use.

2.2.3. Electric field setup for protein loading alignment

For the electric field assisted antibody loading step, we 3D-printed a platform for the copper parallel-plate-based circuit assembly and multi-layered (up to 8 parallel shelves) high-content chip housing (**Figure 2.5A**). In this platform, a relatively uniform electric field intensity of about 43 V/cm is generated in the chip region by applying a DC voltage gradient of 310 V across the parallel plates. COMSOL Multiphysics simulation shows the color map of the electric field between electrode plates in the ZX plane and the plot of the electric field measured along lines stacked in parallel to the X-axis from the bottom shelf to the top shelf (**Figure 2.5B**), and the color map of the electric field between electrode plates in the ZY plane and the plot of the electric field along the Z-axis through the middle section from the bottom shelf to the top shelf (**Figure 2.5C**). The parallel plate electric field platform is powered by an external DC power supply.

2.2.4. Portable reader for the microfluidic Cystatin C paper chip

After the proof-of-concept findings with USB microscope detection, we designed and built a standalone reader (**Figure 2.2A-B; Figure 2.3A**). The main features and components of the reader are a 12 MP camera, a miniature LED backlight, a battery, and a control unit with built-in Wi-Fi and Bluetooth for wireless operation. The control and communication with the reader is performed via a custom Android application. The reader design aims to be as minimalistic as possible for simple and intuitive operation. The reader door with a chip cartridge carrier ensures the correct placement of the cartridge between the camera and RGB backlight.

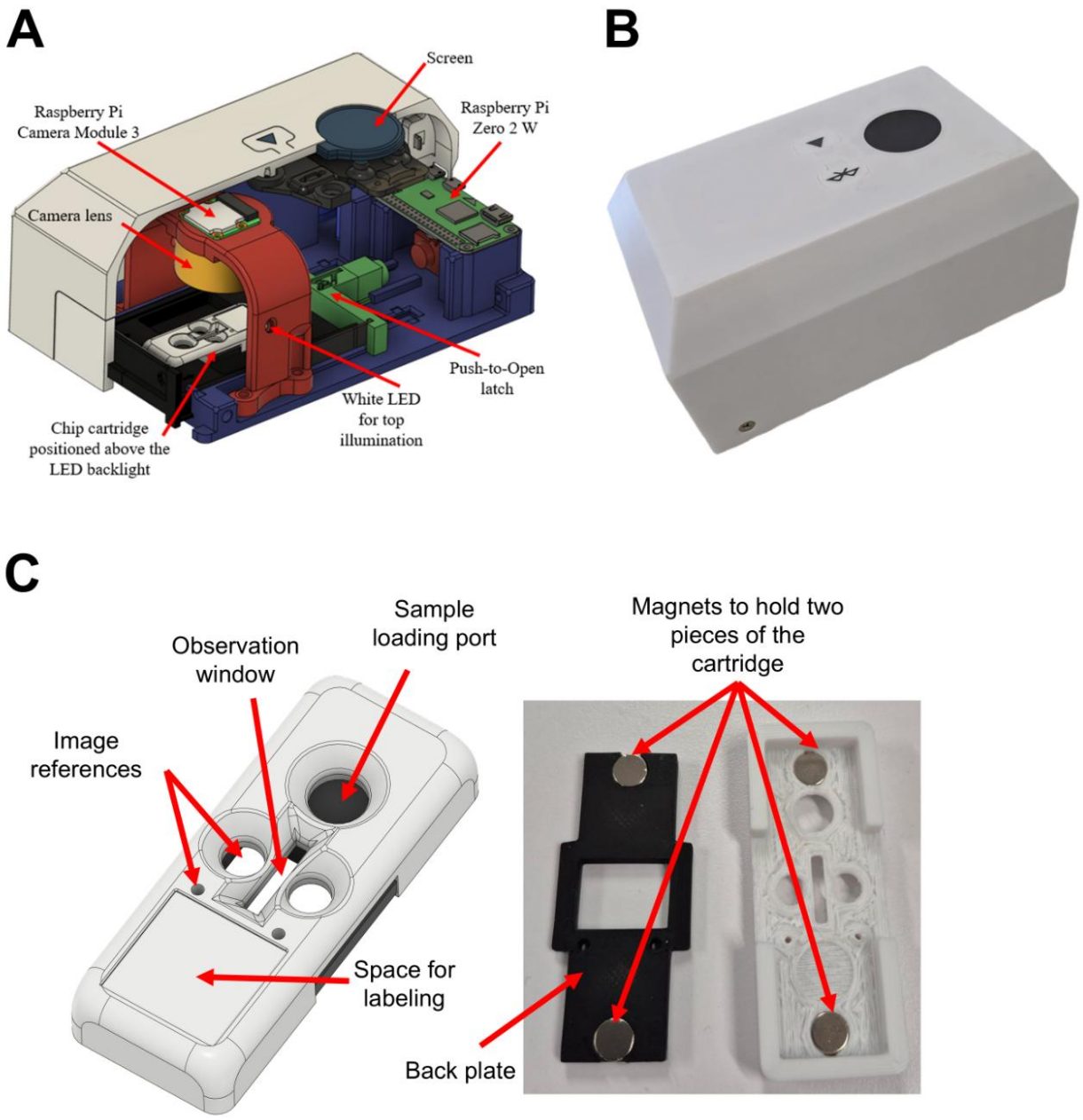

Figure 2.2. portable reader and cartridge for the CYS-C paper chip. A. Illustration of the portable reader design with the open view; B. Closed view of the portable reader; C. Illustration of the 3D printed paper chip cartridge for interfacing with the portable reader (closed view on the left; open view on the right).

2.2.5. Cartridge design and fabrication for the microfluidic Cystatin C paper chip

The paper chip cartridge is designed to hold thin paper chips for ease of use, handling, and proper positioning inside the portable reader (**Figure 2.2C**). The cartridge is assembled from two pieces that are held together by two pairs of magnets. The top part of the cartridge is printed with white PLA, mainly for aesthetic purposes. It has a wide circular port for sample loading and four circular openings used for imaging and cartridge position referencing. The bottom part of the cartridge is printed using black PLA filament to block and absorb the stray light from the backlight.

2.2.6. Smartphone APP for the microfluidic Cystatin C paper chip and the portable reader

A custom Android application was developed capable of transferring the relevant CYC-C data from the portable reader to a smartphone via Bluetooth low-energy (BLE) along with functionality for reading clinically relevant patient data such as sex and age **(Fig 2.3A)**. The Flutter framework (Version 3.24.4) was used for development in combination with Android Studio (Iguana 2023.2.1) to achieve seamless BLE integration and graphical user interface support. The application has three main sections accessible via the bottom navigation bar, which are ‘Home”, “Results”, and “Settings”. The Home tab welcomes the user and initiates whether the portable reader is connected, the settings tab allows the user to connect to the portable reader via BLE, along with the QR code scanning functionality of clinical patient data such as their age and sex, which will automatically calculate eGFR using the data that is sent from the reader. Lastly, the Results tab will show the date of the test, the users age and gender, along with both the measured value of CYS-C and calculated eGFR **(Fig. 2.3A).**

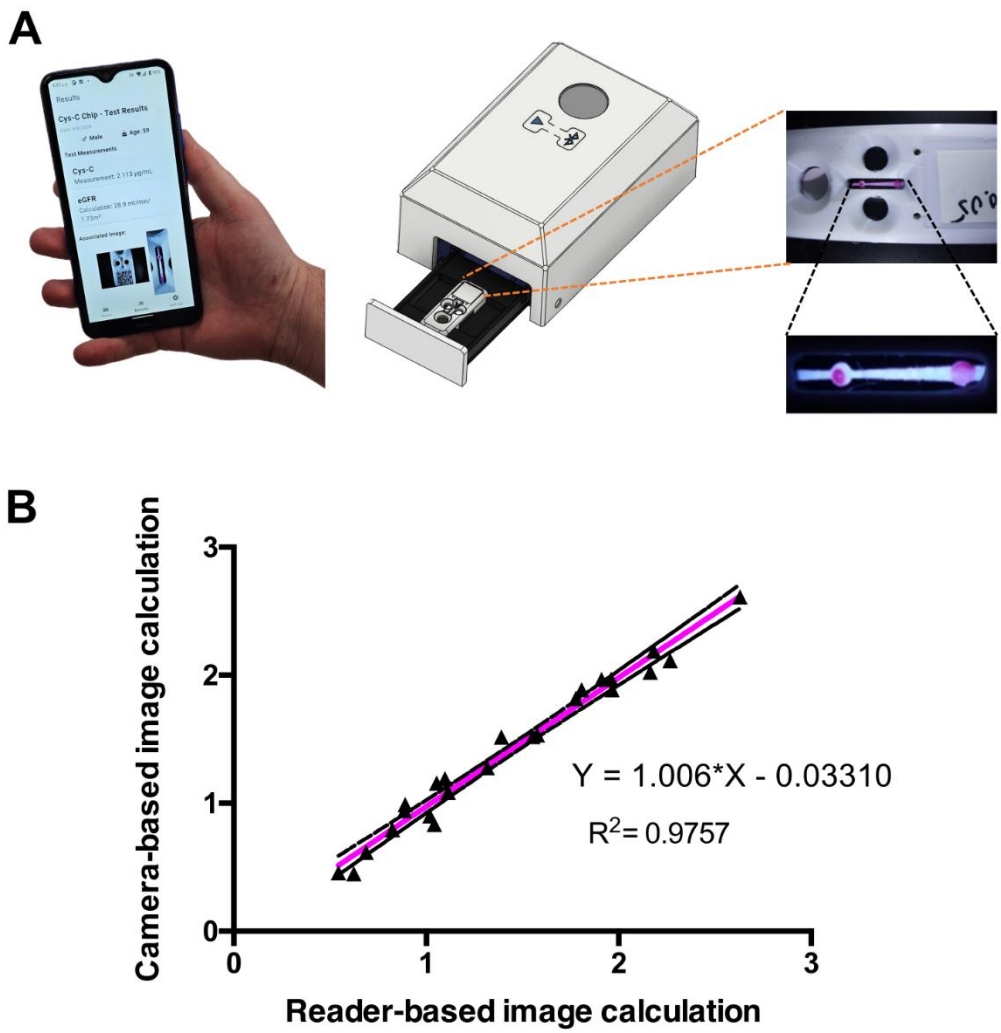

Figure 2.3. The integrated CYS-C paper chip test, the portable reader and smartphone interface application. A. Illustration of the integrated test setup (middle); example test results display on the smartphone app (left); and example color signal from the paper imaged by the portable reader (right); **B.** Comparison of the color signal measurements by the USB microscope and the portable reader.

2.2.7. Microfluidic paper chip test with the Cystatin C standard

For each test, 15 µL CYS-C standard samples for a range of concentrations (i.e. 0.06, 0.055, 0.045, 0.035, 0.03, 0.025, 0.02, 0.015, and 0.01 mg/L spiked in PBS, plus PBS as the blank control) were loaded on the conjugation pad of a new fully prepared chip (**Figure 2.1B**). A few minutes are allowed to pass the test sample fluid from the inlet (conjugation pad) to the outlet (absorbance pad) via capillary action. 15 µL of PBS is then added to the conjugate pad for post-washing. The membrane is allowed to dry at room temperature before image acquisition to detect and quantify the detectable signal. To acquire the images, the paper-based microfluidic device was placed on a stage under a Dino-lite USB Microscope equipped with backlighting, and the magnification is adjusted to isolate the signal points for each test. The USB microscope is connected to an external PC for software control, image acquisition, and analysis.

2.2.8. Microfluidic Cystatin C chip test with clinical serum samples from CKD patients

Serum samples from CKD patients were obtained under an approved ethics protocol by the University of Manitoba. We measured the CYS-C levels in 24 CKD serum samples using the paper chip test. The results from the chip-based tests were further compared with the results obtained from the turbidity assay using the standard well plate format and a conventional plate reader as the reference. Detailed clinical information of the CKD patients, including age, gender, serum creatinine levels, CKD stages based on eGFR, and uACR values, is provided in **Table 2.1**.

The CYS-C paper-based immunoassay chip test was performed on serum from the same 24 CKD patients. Prior to the test, the serum was diluted in PBS at the 1:50 ratio and

then loaded onto the prepared paper chip. After the reaction was completed, the chip channel was allowed to dry at room temperature before imaging to detect and quantify the color signal. Color images captured using a USB microscope were analyzed using ImageJ software for quantitative assessment.

2.3. Data analysis

Image acquisition and colorimetric signal measurement for the paper chip testing was done by capturing a color image with 1280 × 1024 pixels that covers the detection areas by a USB microscope setup equipped with a white background light. One region of interest (ROI) was selected using the "Oval Selections" function from ImageJ software for each detection point of the device. The color signal of each ROI was measured using the "RGB Measure" function from ImageJ and then split into multiple RGB channels, from which the "(R+G+B)/3" channel was used to calculate the signal intensity. The value of "(R+G+B)/3" channel was recorded and deducted by 255 for the color intensity value of each ROI (i.e. Inverted (R+B+G)/3).

Statistical analysis was performed using GraphPad Prism 6.0. Each individual test was repeated at least 3 times. The detection signal data and the CYS-C standard concentrations were interpolated to produce the calibration curves, and the regression was evaluated by the coefficient of determination R^2. For linear regression, the LOD (limit of detection) was calculated as.

$$LOD = 3 \cdot \left(\frac{\sigma}{s}\right)$$

where σ is the standard deviation of the regression intercept and s is the regression slope.

To compare the CYS-C level in the clinical samples measured by the chip test and the reference method, we applied the standard linear regression to evaluate the correlation, and furthermore Bland-Altman analysis, which is a more powerful method to evaluate the variation between the chip test and the reference method [50].

Based on the clinical information of the 24 CKD patients, including age, gender, and serum creatinine levels, we calculated the estimated glomerular filtration rate (eGFR) using the CKD-EPI Creatinine Equation (2021) as follows:

$$eGFRcr = 142 \times \min\left(\frac{Scr}{\kappa}, 1\right)^{\alpha} \times \max\left(\frac{Scr}{\kappa}, 1\right)^{-1.209} \times 0.9938^{Age} [\times 1.012[if\ female]]$$

where: Scr = standardized serum creatinine in mg/dL; κ = 0.7 (females) or 0.9 (males); α = -0.241 (female) or -0.302 (male); min (Scr/κ, 1) is the minimum of Scr/κ or 1.0; max (Scr/κ, 1) is the maximum of Scr/κ or 1.0; Age (years).

For eGFR calculations based on Cystatin C (CYS-C) measurements, we used the CKD-EPI Cystatin C Equation (2012) as follows [25], [51], [52], [53]:

$$eGFR = 133 \times \min\left(\frac{Scys}{0.8}, 1\right)^{-0.499} \times \max\left(\frac{Scys}{0.8}, 1\right)^{-1.328} \times 0.996^{Age} [\times 0.932[if\ female]]$$

where: Scys = standardized serum Cystatin C in mg/L; min is the minimum of Scys/0.8 or 1; max is the maximum of Scys/0.8 or 1; Age (years).

Using the eGFRcr cutoffs for CKD classification (≥60, 30–59, and <30 mL/min/1.73 m²), we categorized the 24 CKD patients into mild, moderate, and severe

kidney damage groups (**Table 2.1**). We then compared the classification accuracy of eGFR predictions derived from paper-based chip tests with the clinical eGFRcr formula-based predictions. The prediction accuracy metrics, including sensitivity, specificity, positive predictive value (PPV), negative predictive value (NPV), and overall accuracy, were calculated using a cross-tabulation table method [54].

Additional materials and methods are provided in the **Materials** and **Methods sections**. No unexpected or unusually high safety hazards were encountered in this study.

2.3.1. Paper-based microfluidic immunoassay chip for Cystatin C measurement

We explored a paper-based microfluidic lateral flow immunoassay (LFIA) to enable more POC-ready quantitative CYS-C test. The initial CYS-C paper chip design included two microfluidic channels linking a common sample inlet to two separate outlets as two parallel repeating test units, each configured with a CYS-C test point and a control point along the respective channel path (**Figure 2.4A**). Averaging the results from the two parallel test units helps balance unit-to-unit test variations while offering a criterion to disqualify the result in case the variation is too high. Using this initial design, our test results achieved a linear range up to 8 mg/L with a LOD of 0.64 mg/L of CYS-C standard spiked in PBS (**Figure 2.4B**), which sufficiently covers the full clinically-relevant serum CYS-C concentration range. However, the LOD of this design requires directly testing the sample without dilution or only allows very limited dilution factors in order to fit the signal into the detection range, especially at the lower end, thus could not effectively address the known high interfering matrix effect in the serum sample.

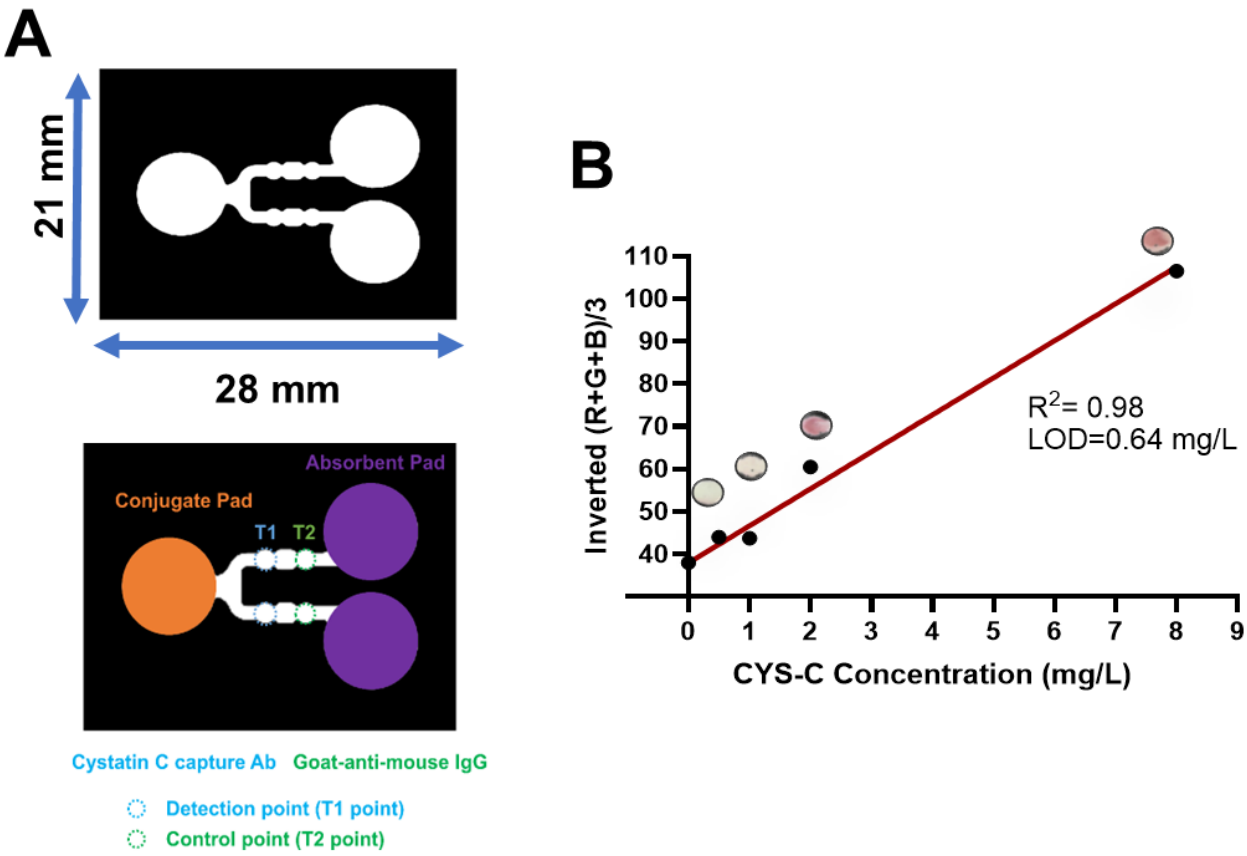

Figure 2.4. Initial design and the preliminary test results of the paper-based microfluidic CYS-C immunoassay chip. A. Illustration of the parallel channel 2-unit design of the CYS-C paper chip is shown; B. The calibration curve of the two-unit design CYS-C paper chip is graphed.

To address this challenge, we hypothesized that optimizing the microfluidic channel design will modulate immunoreaction time and efficiency to achieve a lower LOD, thereby allowing adequate sample dilution. Guided by this hypothesis, we modified the microfluidic paper chip design as follows (**Figure 2.1A**): The microfluidic test channel was designed to have a tapered shape with a narrowing entrance to the T point and broadening exit from the T point toward the C point, and finally a wide and short channel between the C point and the outlet. This tapered channel design would allow for reduced entrance flow to the T point for more efficient antigen capture. As expected, this design achieved significantly enhanced signal intensity in the lower CYS-C concentration range as measured by a USB microscope-based imaging platform (**Figure 2.1C**), which led to a linear range up to at least 0.06 mg/L and a LOD of 0.0033 mg/L (**Figure 2.1B & D**), allowing significant sample dilution (e.g. up to 300X) required to address the matrix effect.

Retrospectively, it is worth mentioning a key issue encountered during our initial design and testing of this new chip before reaching the much-improved results as shown in **Figure 2.1**. Specifically, the new tapered channel design introduced higher unit-to-unit variation, especially when configuring multiple repeating units on a single chip, likely due to the inconsistency of antibody capturing of a smaller amount of antigen molecules and the unevenly divided antigen distribution to different test units from a common sample inlet. To further address this drawback, we first decided to use a single test unit chip in the protocol, thus avoiding the inconsistent antigen dividing issue. Second and more importantly, we focused on improving the capture antibody loading consistency. At a very low loading volume (i.e. a few tens of nL), it is difficult to precisely control the loading

accuracy even with high-precision dispensing equipment. Therefore, we instead invested efforts to improve antibody alignment on the chip, thus aiming to better control antigen capture at the T point and C point with improved consistency or/and efficiency. In this direction, we chose to apply an electric field-based technique to align antibody orientation during the loading process [55], enabled by a 3D printed custom platform for chip housing and electric field application (**Figure 2.5C**). As expected, our results showed the improved linear calibration curve and LOD with the electric field-assisted antibody loading protocol compared to it without the electric field treatment step (i.e. weaker linear regression of the calibration curve, $R^2 = 0.7$; and a lower LOD of 0.027 mg/L) (**Fig. 2.5D**).

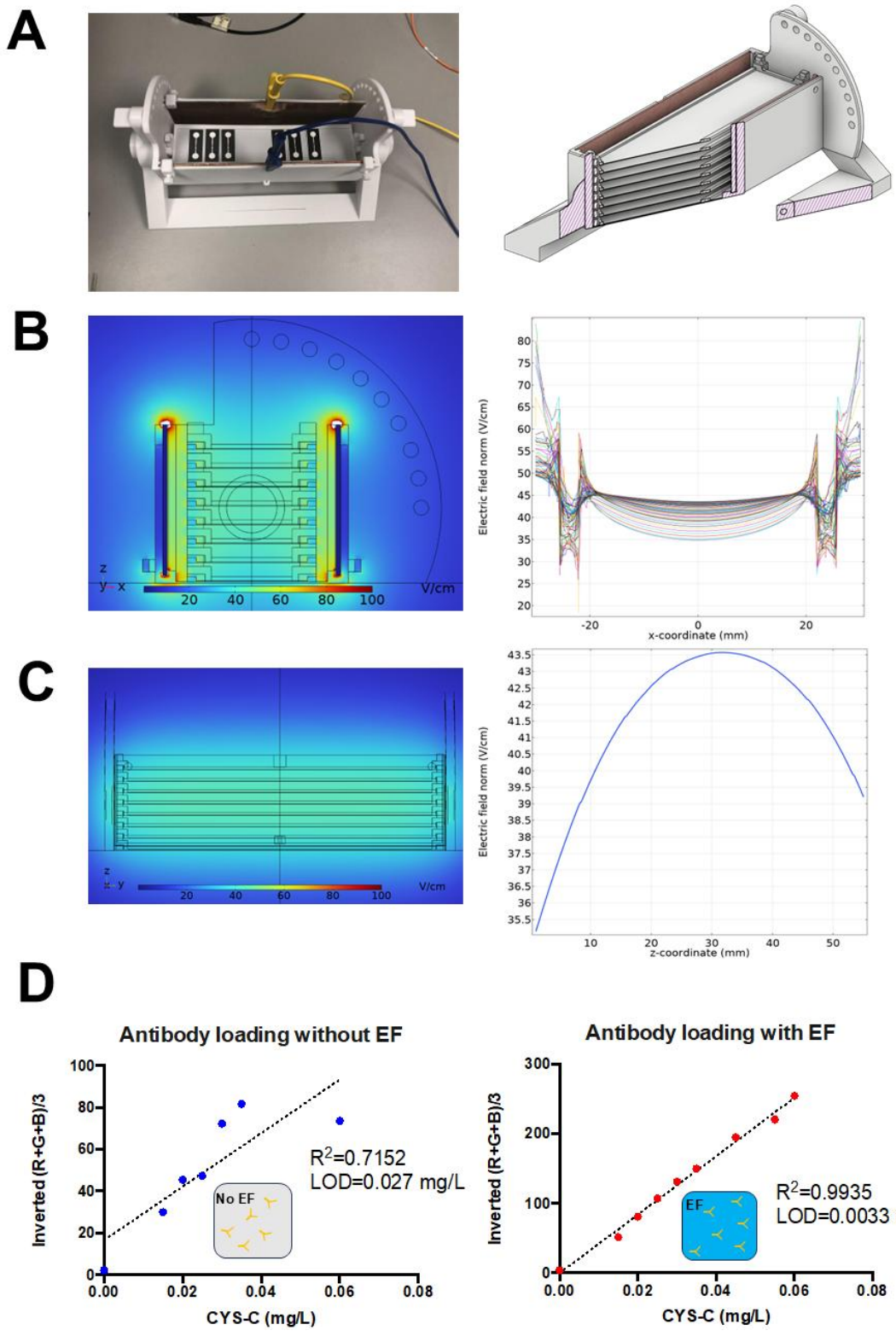

Figure 2.5. Electric field-assisted antibody loading for improved CYS-C paper chip test consistency. A. Illustration of the 3D printed multi-shelf device for electrical

alignment of antibody orientation on the CYS-C paper chips during antibody loading is presented; B. Simulated electric field 2D color map between the parallel electrode plates in the ZX plane (left) and the electric field profile measured along the X-axis at different Z position from the bottom shelf to the top shelf (right) was graphed by COMSOL; C. Simulated electric field 2D color map between the parallel electrode plates in the ZY plane (left) and the electric field profile measured along the Z-axis through the middle section from the bottom shelf to the top shelf (right) are presented; D. Comparison of the calibration curves of the CYS-C paper chip without (left) or with (right) the electric field treatment for antibody loading is highlighted. The inserted diagram illustrates the random antibody orientation (without electric field treatment) vs the aligned antibody orientation (with electric field treatment).

2.3.2. Integrated Cystatin C test with the microfluidic paper chip cartridge and a smartphone-controlled portable colorimetric reader

CYS-C paper chip requires a portable reader to enable POC test applications. In this direction, we developed a compact and low-cost optical reader with dual options of standalone test or wireless-controlled test (**Figure 2.2; 2.3**). The key elements of the reader include a mini RGB backlight, a Raspberry Pi camera module, a wide view lens (120°), and a Raspberry Pi Zero 2W. These components replicate the features of the USB microscope-based imaging platform (**Figure 2.1C**) but in a more compact and integrated format. In addition, we added a number of components and features that are essential for POC test including **1)** a battery and a charging module for truly wireless operation; **2)** a screen for displaying results if the reader is operated as a standalone device; **3)** Bluetooth, Run, and On/Off buttons for essential commands; **4)** additional white LEDs for illuminating the cartridge from the top for QR code scanning and chip orientation checking; **5)** a push-to-open latch door mechanism for an intuitive user interface; and **6)** 3D printed exterior frame and cover of the reader using white filament for esthetic considerations and the interior frame using black filament to reduce light reflections and improve image quality.

To facilitate practical handling of the paper chip by the user and chip interface with the portable reader, we designed and 3D printed a two-piece chip cartridge (**Figure 2.2C**). It features a sample loading port and a rectangular OW that lets the backlight pass through the detection area for further detection and analysis. In addition, the cartridge was configured with several blank holes as the reference background signal reading window and labeling area for QR codes that can store information such as the cartridge type and

expiration date to mimic the real product-like test cartridge appearance and design concept. Similar to the portable reader frame fabrication, the top piece of the cartridge was 3D printed with white PLA filament for esthetic considerations, and the bottom piece was made of black PLA filament to block any stray light that might get through the body of the cartridge. Finally, the two cartridge pieces were aligned with the paper chip in a sandwich fashion and the assembled cartridge was held together tightly by two pairs of magnets. Using the developed portable reader and the chip cartridge, we performed a series of CYS-C paper chip testing that successfully confirmed the identical signal measurement compared with the USB microscope-based platform (**Fig. 2.3B**).

2.3.3. Clinical sample validation of the microfluidic Cystatin C immunoassays for diagnostic test of chronic kidney disease

Based on satisfactory technical calibration of the developed CYS-C paper chip test methods, we performed further validation studies using serum samples from patients who have been diagnosed with CKD. The collected patient data included age, gender, serum CRE (μmol/L), eGFRcr value (eGFR based on the clinically measured serum creatinine level, mL/min/1.73 m^2), uACR (mg/mmol), and CKD stage (**Table 2.1**). The CKD stages were classified based on the eGFRcr values according to the National Collaborating Centre for Chronic Conditions (2008). CKD stages were further grouped into three categories: mild, moderate, and serious kidney function loss. Specifically, the mild kidney damage corresponds to eGFRcr value above 60 mL/min/1.73 m^2 (G1 and G2); the moderate kidney damage includes stages G3a and G3b, with eGFRcr values between 30 and 59 mL/min/1.73 m^2; and the severe kidney damage (stages G4 and G5) is defined by eGFRcr values below

30 mL/min/1.73 m². A total of 24 CKD samples covering these three CKD groups with the eGFRcr range spanned from 18 to 146 mL/min/1.73 m² were tested for chip validation.

Table 2.1. CKD patients' clinical information summary.

ID	Age	Gender	serum CRE (μmol/L)	eGFR (mL/min/1.73m^2)	CDK stage	uACR (mg/mmol)
1	37	F	43.3	124	1 or 2	1.3
2	73	F	49.8	96	1 or 2	2.2
3	56	M	51.3	114	1 or 2	7
4	21	F	33.7	146	1 or 2	3.4
5	71	F	58.9	94	1 or 2	4
6	52	M	85.2	95	1 or 2	0.7
7	52	M	75.2	105	1 or 2	3.6
8	59	F	78.3	75	1 or 2	7.5
9	49	M	70.8	108	1 or 2	26
10	60	M	83	93	1 or 2	22.4
11	67	M	106.5	66	1 or 2	0.9
12	71	F	117.2	43	3a	8.3
13	74	M	124	53	3a	4.2
14	78	F	105	47	3b	22.9
15	74	F	100.7	51	3a	36.2
16	76	M	162.4	38	3b	0.4
17	59	M	188.4	35	3b	7
18	72	M	207.1	29	4	3.2
19	72	M	160.4	39	3b	28.9
20	35	M	180.4	43	3b	30.1
21	88	M	253.3	20	4	10.7
22	56	M	247.2	26	4	16.6
23	72	M	291.2	19	4	31
24	73	F	237	18	4	128.9

Level of Kidney Disease	CKD Stage	eGFR Value
Mild	G1	≥90
	G2	60-89
Moderate	G3a	45-59
	G3b	30-44
Severe	G4	15-29
	G5	≤15

The general trend of the inverse proportionality between the filtration markers (i.e. clinically determined serum creatinine or chip-measured serum CYS-C) and their respective eGFR based on the filtration marker specific estimation formula was first verified in these clinical CKD samples (**Figure 2.6**). Next, as a primary technical validation measure, we quantitatively compared the chip test results of CYS-C for these 24 CKD serum samples to a reference test method (turbidimetric well test). Instead of the conventional linear regression-based correlation analysis, we applied the well-established and considerably more effective Bland-Altman (B-A) analysis [56] to assess the system bias between the chip measurements and the reference immunoturbidity assay in the standard well-plate format. In the B-A analysis, the difference between the two methods was plotted against the average of the two measurements. Our results showed that for the paper chip test, the mean difference is slightly more than 1 mg/L (1.274 mg/L for the paper chip) and most of the test data falls within the limit-of-agreement (LoA), which is calculated as the 95% confidence intervals (i.e. +/- 1.96 times the standard deviation of the mean difference) (**Figure 2.7**). In the context of CKD, serum CYS-C levels above 0.95 mg/L typically indicate impaired kidney function, while levels below 0.95 mg/L are generally considered within the normal range [57]. A survey of 141 laboratories reported mean CYS-C values for CKD samples ranging from 2.052-2.909, highlighting significant variability and high biases across different lab tests [58], [59]. Therefore, given the mean bias and the data spread around the mean bias according to the B-A analysis, we next designed our secondary analysis to evaluate the CKD stage prediction accuracy based on the chip test and the CKD-EPI Cystatin C Equation for eGFR against the clinical eGFRcr values as the comparison reference.

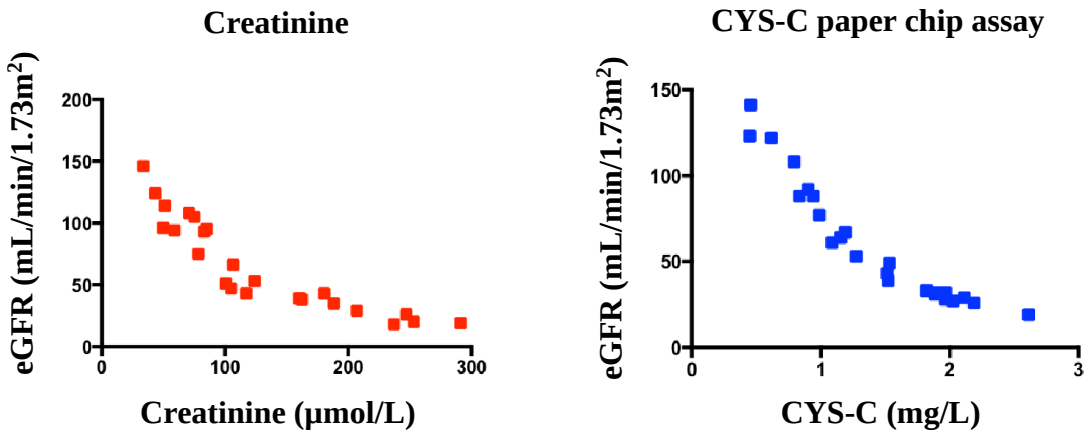

Figure 2.6. Declining trend of eGFR against the respective serum filtration marker based on the filtration marker specific estimation formula using the 24 clinical CKD samples. Left. eGFR vs clinically measured serum creatinine; **Right.** eGFR vs paper chip method.

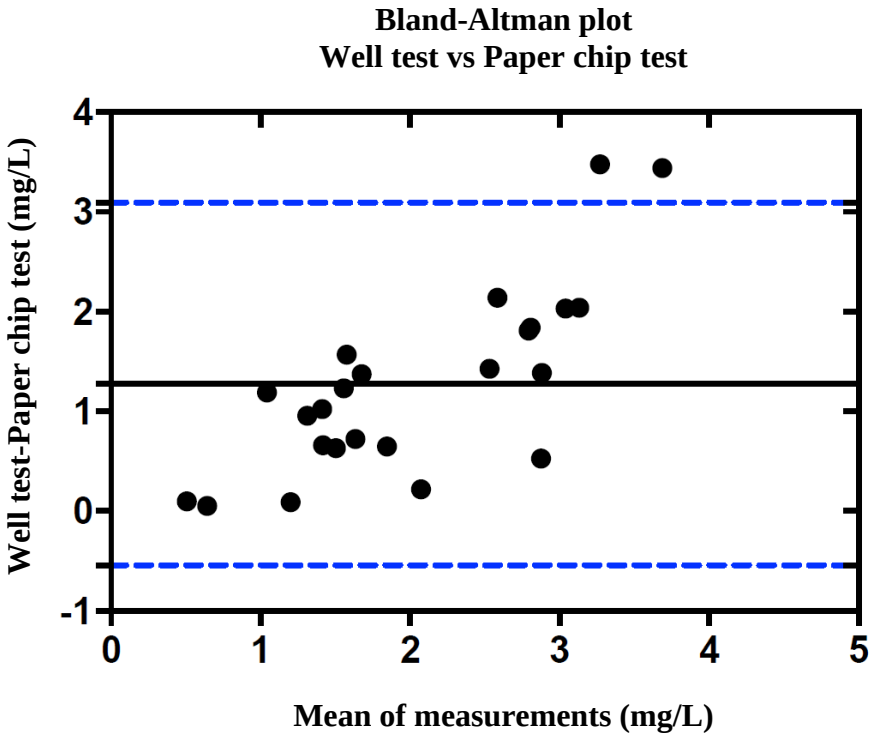

Figure 2.7. Bland-Altman analysis of the proposed test setups vs well testing.

Proceeding with the CKD stage prediction accuracy analysis, we first applied a simple binary approach to evaluate the eGFR prediction accuracy based on our CYS-C chip tests (eGFRcys-c) against the clinically-determined eGFRcr values as the hypothetical ground truth. Clinically, an eGFRcr of 90 mL/min/1.73 m² or higher is considered normal; an eGFRcr below 60 mL/min/1.73 m² indicates kidney disease; and an eGFRcr below 15 mL/min/1.73 m² signifies kidney failure. Thus, we analyzed the diagnostic accuracy of our CYS-C chip test to distinguish between normal and CKD using the cutoff eGFRcr 60 mL/min/1.73 m². **Table 2.2** summarizes the binary-based prediction accuracy evaluators, including sensitivity, specificity, positive predictive value (PPV), negative predictive value (NPV), and overall accuracy. Among the 24 clinical samples, 22 samples were correctly predicted using the CYS-C paper chip (accuracy: 92%). These results motivated us to further evaluate the prediction accuracy at higher resolution. Specifically, we analyzed the prediction accuracy of the chip test based on the three CKD stage categories as defined in **Table 2.1**. Our results showed that the paper chip test achieved relatively high accuracy (> 80%) in classifying patients with eGFRcr > 60 or < 30 mL/min/1.73 m² for the mild or server stage respectively, whereas the prediction accuracy for the moderate CKD stage (eGFRcr 30–59 mL/min/1.73 m²) is lower (<80%) as expected (**Table 2.3**).

Table 2.2. Serum CYS-C eGFR diagnosis accuracy with the cross-tabulation table comparison with an eGFR from serum CRE.

		Clinical eGFR (serum CRE)		
		Positive	**Negative**	**Total**
CYS-C Paper chip	**Positive**	12	1	13
	Negative	1	10	11
	Total	13	11	24

	Sensitivity	**Specificity**	**PPV**	**NPV**	**Accuracy**
CYS-C Paper chip	92%	91%	92%	91%	92%

Table 2.3.Three-stage (mild, moderate and severe) eGFR diagnosis accuracy based on the CYS-C chip test using the 24 clinical CKD samples.

The cross-tabulation table for pairs of serum CYS-C eGFR level >60, 30-59, <30ml/min/1.73m^2 and the reference standard of an eGFR from serum CRE

			clinical eGFR (serum CRE)		
			Positive	**Negative**	**Total**
CYS-C Paper chip tests	eGFR > 60	**Positive**	10	1	11
		Negative	1	12	13
		Total	11	13	24
	eGFR 30-59	**Positive**	5	3	8
		Negative	3	13	16
		Total	8	16	24
	eGFR <30	**Positive**	3	2	5
		Negative	2	17	19
		Total	5	19	24

Diagnostic accuracy of the paper chip results detections of eGFR >60, 30-59, <30ml/min/1.73m^2

		Sensitivity	Specificity	PPV	NPV	Accuracy
CYS-C Paper chip tests	eGFR > 60 ml/min/1.73m2	91%	92%	91%	92%	92%
	eGFR is 30-59 ml/min/1.73m2	63%	81%	63%	81%	75%
	eGFR < 30 ml/min/1.73m2	60%	89%	60%	89%	83%

Top. Cross-tabulation table comparing the CYS-C chip predicted eGFRcys-C against the clinical creatinine predicted eGFRcr is shown; **Bottom.** The accuracy evaluators based on data in the Top table, including the sensitivity, specificity, PPV, NPV, and overall accuracy, are shown.

2.4. Discussion

In this study, we developed a microfluidic solution for POC measurement of serum CYS-C as an important diagnostic biomarker for CKD. Among the few reported paper-based non-microfluidic lateral flow immunoassay (LFIA) for CYS-C measurement, an earlier study used fluorescence-tagged detection antibody to achieve an impressive wide detection range and the LOD of 0.023 mg/L of CYS-C standard spiked in urine samples, although urine CYS-C is not an established diagnostic biomarker for CKD, and fluorescent signal detection is considerably more complicated [60]. A more recent work described a similar paper-based LFIA but used the standard gold-nanoparticle conjugated detection antibody and applied the assay for straightforward colorimetric quantification of CYS-C in human blood samples. This assay achieved the full clinically-relevant detection range of 0.5-7.5 mg/L and the LOD of 0.18 mg/L without requiring sample dilution [61]. Although the assay directly addressed the matrix interference effect, it inevitably came with the drawback of establishing the calibration curve using CYS-C standard spiked in endogenous CYS-C depleted blood samples, which would intrinsically introduce calibration sample variations. Compared to these previous developments, our CYS-C paper chip integrated its useful features in effective LFIA chemistry and optical signal measurement while balancing its limitations by incorporating microfluidic controls to realize the clinically practical blood CYS-C test in POC settings with minimized matrix interference and the desired quantitative accuracy.

Previous studies have demonstrated the superior performance of CYS-C-based eGFR determination in specific patient populations [62]. For instance, in renal transplant recipients, $eGFR_{CYS\text{-}C}$ was found to be more accurate than traditional creatinine-based

equations [63]. Similar findings were reported in patients with rheumatoid arthritis and secondary amyloidosis [64] and cirrhotic patients [65]. Additionally, studies have suggested that eGFR determination can be further improved by incorporating both creatinine and CYS-C values [66]. Indeed, the CKD-EPI Creatinine-Cystatin C Equation (2021), which integrates serum CYS-C levels, serum creatinine levels, age, gender and race led to more accurate eGFR [67]. In this context, our developed CYS-C chip tests provide the POC diagnostic tool required for improved eGFR determination in CKD and furthermore have the potential to enable integrated tests of the dual eGFR markers based on CYS-C and creatinine on a single microfluidic chip.

Most commonly used CYS-C assays include ELISA and immunoturbidity assay, with the latter to be also being the current standard clinical lab test [68]. Both methods require specialized lab facilities and skills. The ELISA test kit is typically over several hundred dollars in cost, while the immunoturbidity assay-based clinical test costs over $30 per test and often needs long-distance sample transport. According to a 2019 survey by the College of American Pathologists, only 7% of US clinical laboratories offered CYS-C tests [68], [69] and clinical POC CYS-C test is currently not available. In this context, our developed CYS-C chip tests present clear technical and practical advantages over the existing test methods (**Table 2.4**). For the ideal sample-to-result POC CYS-C test, on-chip serum or plasma isolation from whole blood is required, which we have demonstrated such practical feasibility in our previously developed C-reactive protein test chip (CRP-Chip) with the integrated plasma isolation membrane [70]. Collectively, our CYS-C chip tests represent a transformative POC solution to realize the advantageous use of CYS-C for CKD diagnosis, risk monitoring and therapeutic management.

Table 2.4. Comparison of the paper chip with selected commercial CYS-C test

	ELISA	Turbidity assay	CYS-C paper chip
Detection	colorimetric	turbidity	colorimetric
Reaction	sandwich immunoassay	immunoturbidimetry	sandwich immunoassay
Sample volume	100 µL	1.5 µL	1 µL
LOD	10 pg/mL	0.3 mg/L	0.003 mg/L
Detection range	0.312~20 ng/mL	0.5~8.0 mg/L	0.01~0.06 mg/L
Assay duration	4.5 hrs	~20 mins	~20 mins
Cost (CAD)	~$20 / sample	~$20 / sample	< $0.7 / test
User skills level	high	high	low
Portable reader	no	no	yes
Suitable for POC	no	no	yes

Chapter 3: Conclusion and outlook

3.1. Summary of key findings and significance of the work

In this comprehensive study, the adaptability of paper-based microfluidics to lateral flow immunoassay methods has been explored. As discussed, lateral flow immunoassays are mainly utilized in qualitative measurements, however, quantitative LFIAs are proposed in research setups. In the context of CKD biomarkers and CYS-C specifically, a number of assays have been developed, but they either require fluorescent spectroscopy [71] or the limit of detection is noticeably high in the way that dilution is not possible. Testing real clinical samples presents challenges due to matrix complexity, which can cause background interference and increase the likelihood of false positives or negatives. One effective solution would be high dilution factor that mitigates this chance of interference. Our developed paper-based microfluidic platform not only allows for up to 300X dilution but also has the fraction of the cost for fabrication and data recording. This high level of precision and accuracy is derived from a precisely engineered microfluidic layout and an integrated electric field-enhancement strategy.

3.2. Comparison to existing technologies

In the past decade, several point-of-care technologies have been developed to satisfy the need for rapid and accurate CKD biomarker testing. While there are several examples of urine POC platforms that analyze different components of urine samples for CKD, affordable and accurate options for blood biomarkers are in need. Abbott i-STAT 1 System a point-of-care system that promises clinical-lab-level quality for blood biomarkers, has a price point of just below 5000 USD. The main component of this platform is the portable analyzer capable of performing signal analysis on specialized cartridges. The CKD target biomarker options are limited to blood creatinine, which does

not satisfy the need for clinicians in diagnosis and disease progression analysis [72]. Abaxis company offers kidney-focused cartridges for its Piccolo Xpress platform, featuring CKD urine and blood biomarkers such as albumin and creatinine. This platform, however, suffers from the same problems: high price point and not covering CYS-C as a preferred biomarker. The mentioned platforms are made to be used in clinical settings, and personal use will lead to a number of complications, such as required training, personal errors and financial burden for individuals.

Many commercial POCT platforms with quantitative capabilities restrict direct reporting of numerical results due to regulatory constraints. Consumer-oriented devices like U-Scan lack clinical precision and underscore the need for diagnostic-grade POC tools [73]. The result of the analysis is mainly focused on providing general recommendations. DCA Vantage [74], a platform able to analyze customized test cartridges, is an example of a clinically approved POCT device with the possibility of used by individuals. Being designed for urgent care rooms, this platform measures uACR biomarker and provides 3 measurements for urine samples, urine creatinine, urine albumin, and their ratio. Considering these features, this option can be reliably used for CKD screening. The convenience of current POCT platforms comes with caveats. DCA Vantage has a price point of over 5000 USD, training is required, urine biomarkers do not provide a clear view for CKD, and cartridges are far more expensive than our designed test chips.

3.3. Future directions

In this study, we discovered the potential of one testing method, LFIA, to analyze a CKD biomarker. Considering the available anti-HSA antibodies, this method could be

expanded to HSA (Human Serum Albumin) analysis to contribute to risk factor analysis. Another possibility is the idea of multiplexed chips, meaning that a microfluidic chip with multiple channels and a test point for total analysis of real samples.

The standard diagnostics and screening process relies on an analysis of different biomarkers and consideration of different factors. An ideal diagnostic tool for clinicians is the one capable of quantifying several analytes, showcasing proper classification. Multiplexed point-of-care testing (xPOCT) is the potential solution, and microfluidics has shown great adaptability to this application. Paper-based microfluidic devices have presented ideal flexibility for multiple-biomarker diagnostic tests. One design would be placing multiple channels between the inlet and outlet of a lateral flow immunoassay, each containing CKD biomarker antibodies, performing simultaneous analysis from one sample. More basic designs have been reported, for example, defining circular reaction zones on a single paper chip [75]. Employing this principle, multiplexed systems are designed to satisfy affordable screening methods for underprivileged communities [76]. In the case of chronic kidney disease, there are a number of reference biomarkers, such as urine creatinine, urine albumin, CYS-C, and inflammation-involved proteins. The future possible work is to include a sufficient number of biomarkers in the form of paper-based LFIA. Although this approach has complications in terms of fabrication, it is an ideal direction for diagnostic lab-on-a-chip research. Future work will aim to integrate these biomarkers into a unified, low-cost diagnostic chip suitable for both clinical and decentralized settings.

References

[1] M. R. Pollak, S. E. Quaggin, M. P. Hoenig, and L. D. Dworkin, “The Glomerulus: The Sphere of Influence,” *Clin J Am Soc Nephrol*, vol. 9, no. 8, p. 1461, 2014, doi: 10.2215/CJN.09400913.

[2] S. Lopez-Giacoman and M. Madero, “Biomarkers in chronic kidney disease, from kidney function to kidney damage,” *World J Nephrol*, vol. 4, no. 1, p. 57, 2015, doi: 10.5527/WJN.V4.I1.57.

[3] S. Altamura, D. Pietropaoli, F. Lombardi, R. Del Pinto, and C. Ferri, “An Overview of Chronic Kidney Disease Pathophysiology: The Impact of Gut Dysbiosis and Oral Disease,” *Biomedicines*, vol. 11, no. 11, p. 3033, Nov. 2023, doi: 10.3390/BIOMEDICINES11113033.

[4] C. Zoccali *et al.*, “The systemic nature of CKD,” Jun. 01, 2017, *Nature Publishing Group*. doi: 10.1038/nrneph.2017.52.

[5] P. E. Stevens *et al.*, “KDIGO 2024 Clinical Practice Guideline for the Evaluation and Management of Chronic Kidney Disease,” *Kidney Int*, vol. 105, no. 4, pp. S117–S314, Apr. 2024, doi: 10.1016/J.KINT.2023.10.018/ASSET/210CFA23-1B32-495D-BD2B-45CB202E6E90/MAIN.ASSETS/GR10.JPG.

[6] A. Tojo and S. Kinugasa, “Mechanisms of glomerular albumin filtration and tubular reabsorption,” *Int J Nephrol*, vol. 2012, 2012, doi: 10.1155/2012/481520,.

[7] V. Lekskulchai, “Use of Estimated Glomerular Filtration Rate and Urine Albumin-to-Creatinine Ratio Based on KDIGO 2012 Guideline in a Thai Community Hospital: Prevalence of Chronic Kidney Disease and its Risk Factors,” *Med Sci Monit Basic Res*, vol. 28, p. e938176, Dec. 2022, doi: 10.12659/MSMBR.938176.

[8] J. C. Seegmiller and L. M. Bachmann, “Urine Albumin Measurements in Clinical Diagnostics,” *Clin Chem*, vol. 70, no. 2, pp. 382–391, Feb. 2024, doi: 10.1093/CLINCHEM/HVAD174.

[9] S. W. Benoit, E. A. Ciccia, and P. Devarajan, “Cystatin C as a biomarker of chronic kidney disease: latest developments,” *Expert Rev Mol Diagn*, vol. 20, no. 10, pp. 1019–1026, 2020, doi: 10.1080/14737159.2020.1768849.

[10] C. P. Price, “Point of care testing,” *BMJ : British Medical Journal*, vol. 322, no. 7297, p. 1285, May 2001, doi: 10.1136/BMJ.322.7297.1285.

[11] K. J. Land, D. I. Boeras, X. S. Chen, A. R. Ramsay, and R. W. Peeling, “REASSURED diagnostics to inform disease control strategies, strengthen health systems and improve patient outcomes,” *Nat Microbiol*, vol. 4, no. 1, pp. 46–54, Jan. 2019, doi: 10.1038/S41564-018-0295-3;SUBJMETA=107,1856,2522,255,326,631,692,699;KWRD=APPLIED+MICROBIOLOGY,CLINICAL+MICROBIOLOGY,TUBERCULOSIS.

[12] B. G. Andryukov, “Six decades of lateral flow immunoassay: from determining metabolic markers to diagnosing COVID-19,” *AIMS Microbiol*, vol. 6, no. 3, p. 280, 2020, doi: 10.3934/MICROBIOL.2020018.

[13] A. K. Yetisen, M. S. Akram, and C. R. Lowe, “Paper-based microfluidic point-of-care diagnostic devices,” *Lab Chip*, vol. 13, no. 12, p. 2210, 2013, doi: 10.1039/c3lc50169h.

[14] Anushka, A. Bandopadhyay, and P. K. Das, “Paper based microfluidic devices: a review of fabrication techniques and applications,” *Eur Phys J Spec Top*, vol. 232, no. 6, p. 781, Jun. 2022, doi: 10.1140/EPJS/S11734-022-00727-Y.

[15] A. C. Webster, E. V Nagler, R. L. Morton, and P. Masson, “Chronic Kidney Disease,” *The Lancet*, vol. 389, no. 10075, pp. 1238–1252, Mar. 2017, doi: 10.1016/S0140-6736(16)32064-5.

[16] A. Francis *et al.*, “Chronic kidney disease and the global public health agenda: an international consensus,” *Nat Rev Nephrol*, vol. 20, no. 7, pp. 473–485, Jul. 2024, doi: 10.1038/s41581-024-00820-6.

[17] K. J. Jager, C. Kovesdy, R. Langham, M. Rosenberg, V. Jha, and C. Zoccali, “A single number for advocacy and communication—worldwide more than 850 million individuals have kidney diseases,” *Nephrology Dialysis Transplantation*, vol. 34, no. 11, pp. 1803–1805, Nov. 2019, doi: 10.1093/ndt/gfz174.

[18] M. Jadoul, M. Aoun, and M. Masimango Imani, “The major global burden of chronic kidney disease,” *Lancet Glob Health*, vol. 12, no. 3, pp. e342–e343, Mar. 2024, doi: 10.1016/S2214-109X(24)00050-0.

[19] R. Kazancioğlu, “Risk factors for chronic kidney disease: an update,” *Kidney Int Suppl (2011)*, vol. 3, no. 4, pp. 368–371, Dec. 2013, doi: 10.1038/kisup.2013.79.

[20] M. J. Dobrow, V. Hagens, R. Chafe, T. Sullivan, and L. Rabeneck, “Consolidated principles for screening based on a systematic review and consensus process,” *Can Med Assoc J*, vol. 190, no. 14, pp. E422–E429, Apr. 2018, doi: 10.1503/cmaj.171154.

[21] J. M. G. J. G. & W. H. Organization. Wilson, *Principles and practice of screening for disease*. 1968.

[22] A. M. Foudeh, T. Fatanat Didar, T. Veres, and M. Tabrizian, “Microfluidic designs and techniques using lab-on-a-chip devices for pathogen detection for point-of-care diagnostics,” *Lab Chip*, vol. 12, no. 18, p. 3249, 2012, doi: 10.1039/c2lc40630f.

[23] L. Gervais, N. de Rooij, and E. Delamarche, “Microfluidic Chips for Point-of-Care Immunodiagnostics,” *Advanced Materials*, vol. 23, no. 24, Jun. 2011, doi: 10.1002/adma.201100464.

[24] L. Syedmoradi and F. A. Gomez, “Paper-Based Point-Of-Care Testing in Disease Diagnostics,” *Bioanalysis*, vol. 9, no. 11, pp. 841–843, Jun. 2017, doi: 10.4155/bio-2017-0080.

[25] L. A. Inker *et al.*, “Estimating Glomerular Filtration Rate from Serum Creatinine and Cystatin C,” *New England Journal of Medicine*, vol. 367, no. 1, pp. 20–29, Jul. 2012, doi: 10.1056/NEJMoa1114248.

[26] Lijo B., “Creatinine Test vs Cystatin C Test.,” AGAPPE. agappe.com/swiss_en/blog-details/creatinine-test-vs-cystatin-c-test.html.

[27] C. Delgado *et al.*, “A Unifying Approach for GFR Estimation: Recommendations of the NKF-ASN Task Force on Reassessing the Inclusion of Race in Diagnosing Kidney Disease,” *Journal of the American Society of Nephrology*, vol. 32, no. 12, pp. 2994–3015, Dec. 2021, doi: 10.1681/ASN.2021070988.

[28] C. Delgado *et al.*, “A Unifying Approach for GFR Estimation: Recommendations of the NKF-ASN Task Force on Reassessing the Inclusion of Race in Diagnosing Kidney Disease,” *American Journal of Kidney Diseases*, vol. 79, no. 2, pp. 268-288.e1, Feb. 2022, doi: 10.1053/j.ajkd.2021.08.003.

[29] L. A. Inker *et al.*, “New Creatinine- and Cystatin C–Based Equations to Estimate GFR without Race,” *New England Journal of Medicine*, vol. 385, no. 19, pp. 1737–1749, Nov. 2021, doi: 10.1056/NEJMoa2102953.

[30] H. J. Kramer, B. G. Jaar, M. J. Choi, P. M. Palevsky, J. A. Vassalotti, and M. V. Rocco, “An Endorsement of the Removal of Race From GFR Estimation Equations: A Position Statement From the National Kidney Foundation Kidney Disease Outcomes Quality Initiative,” *American Journal of Kidney Diseases*, vol. 80, no. 6, pp. 691–696, Dec. 2022, doi: 10.1053/j.ajkd.2022.08.004.

[31] J. Helmersson-Karlqvist *et al.*, “Cystatin C predicts long term mortality better than creatinine in a nationwide study of intensive care patients,” *Sci Rep*, vol. 11, no. 1, p. 5882, Mar. 2021, doi: 10.1038/s41598-021-85370-8.

[32] G. Kaur and E. Levy, “Cystatin C in Alzheimer’s disease,” *Front Mol Neurosci*, vol. 5, 2012, doi: 10.3389/fnmol.2012.00079.

[33] P. M. Mathews and E. Levy, “Cystatin C in aging and in Alzheimer’s disease,” *Ageing Res Rev*, vol. 32, pp. 38–50, Dec. 2016, doi: 10.1016/j.arr.2016.06.003.

[34] S. W. van der Laan *et al.*, “Cystatin C and Cardiovascular Disease,” *J Am Coll Cardiol*, vol. 68, no. 9, pp. 934–945, Aug. 2016, doi: 10.1016/j.jacc.2016.05.092.

[35] Y. Xu, Y. Ding, X. Li, and X. Wu, “Cystatin C is a disease-associated protein subject to multiple regulation,” *Immunol Cell Biol*, vol. 93, no. 5, pp. 442–451, May 2015, doi: 10.1038/icb.2014.121.

[36] M. Zi and Y. Xu, “Involvement of cystatin C in immunity and apoptosis,” *Immunol Lett*, vol. 196, pp. 80–90, Apr. 2018, doi: 10.1016/j.imlet.2018.01.006.

[37] S. K. Bikkarolla, K. Venkatesan, Y. R. Revathy, S. Parameswaran, S. Krishnakumar, and D. Dendukuri, “The Quantitative Detection of Cystatin-C in Patient Samples Using a Colorimetric Lateral Flow Immunoassay,” *Biosensors (Basel)*, vol. 14, no. 1, p. 30, Jan. 2024, doi: 10.3390/bios14010030.

[38] J. Tao, P. Zhao, and Q. Zeng, “The determination of cystatin C in serum based on label-free and near-infrared light emitted PbS@BSA QDs,” *J Mater Chem B*, vol. 4, no. 24, pp. 4258–4262, 2016, doi: 10.1039/C6TB00080K.

[39] S. Ujvari, C. C. Schwarzwald, N. Fouché, J. Howard, and A. Schoster, “Validation of a Point-of-Care Quantitative Equine IgG Turbidimetric Immunoassay and Comparison of IgG Concentrations Measured with Radial Immunodiffusion and a Point-of-Care IgG <scp>ELISA</scp>,” *J Vet Intern Med*, vol. 31, no. 4, pp. 1170–1177, Jul. 2017, doi: 10.1111/jvim.14770.

[40] F. Li *et al.*, “Paper-based point-of-care immunoassays: Recent advances and emerging trends,” *Biotechnol Adv*, vol. 39, p. 107442, Mar. 2020, doi: 10.1016/j.biotechadv.2019.107442.

[41] S. Park, Y. Zhang, S. Lin, T.-H. Wang, and S. Yang, “Advances in microfluidic PCR for point-of-care infectious disease diagnostics,” *Biotechnol Adv*, vol. 29, no. 6, pp. 830–839, Nov. 2011, doi: 10.1016/j.biotechadv.2011.06.017.

[42] T. Chakraborty, M. Das, C. Y. Lin, and C. H. Kao, “Electrochemical detection of cystatin C by oriented antibody immobilization on streptococcal protein G–modified ZIF-8-Cu1−xNix(OH)2@Cu core-shell nanostructured electrode,” *Mater Today Chem*, vol. 27, p. 101273, Jan. 2023, doi: 10.1016/j.mtchem.2022.101273.

[43] E. K. G. Trindade, B. V. M. Silva, and R. F. Dutra, “A probeless and label-free electrochemical immunosensor for cystatin C detection based on ferrocene functionalized-graphene platform,” *Biosens Bioelectron*, vol. 138, p. 111311, Aug. 2019, doi: 10.1016/j.bios.2019.05.016.

[44] M. Xia *et al.*, “Highly Efficient Photoelectrochemical Detection of Cystatin C Based on a Core–Shell MOF Nanocomposite with Biomimetic-Catalysis Amplification,” *ACS Omega*, vol. 9, no. 26, pp. 28228–28236, Jul. 2024, doi: 10.1021/acsomega.4c01644.

[45] P. Coliaie *et al.*, “Machine Learning-Driven, Sensor-Integrated Microfluidic Device for Monitoring and Control of Supersaturation for Automated Screening of Crystalline Materials,” *ACS Sens*, vol. 7, no. 3, pp. 797–805, Mar. 2022, doi: 10.1021/acssensors.1c02358.

[46] L. J. Lucas, J.-H. Han, J. Chesler, and J.-Y. Yoon, “Latex immunoagglutination assay for a vasculitis marker in a microfluidic device using static light scattering detection,” *Biosens Bioelectron*, vol. 22, no. 9–10, pp. 2216–2222, Apr. 2007, doi: 10.1016/j.bios.2006.10.029.

[47] M. Dong *et al.*, “Rapid and Low-Cost CRP Measurement by Integrating a Paper-Based Microfluidic Immunoassay with Smartphone (CRP-Chip),” *Sensors*, vol. 17, no. 4, p. 684, Mar. 2017, doi: 10.3390/s17040684.

[48] D. R. Hristov, C. Rodriguez-Quijada, J. Gomez-Marquez, and K. Hamad-Schifferli, “Designing Paper-Based Immunoassays for Biomedical Applications,” *Sensors*, vol. 19, no. 3, p. 554, Jan. 2019, doi: 10.3390/s19030554.

[49] D. Lin *et al.*, "A novel polymer-based nitrocellulose platform for implementing a multiplexed microfluidic paper-based enzyme-linked immunosorbent assay," *Microsyst Nanoeng*, vol. 8, no. 1, p. 53, May 2022, doi: 10.1038/s41378-022-00385-z.

[50] D. Giavarina, "Understanding Bland Altman analysis," *Biochem Med (Zagreb)*, vol. 25, no. 2, pp. 141–151, 2015, doi: 10.11613/BM.2015.015.

[51] A. Grubb, S. Blirup-Jensen, V. Lindström, C. Schmidt, H. Althaus, and I. Zegers, "First certified reference material for cystatin C in human serum ERM-DA471/IFCC," *cclm*, vol. 48, no. 11, pp. 1619–1621, Nov. 2010, doi: 10.1515/CCLM.2010.318.

[52] C. A. Peralta, "Detection of Chronic Kidney Disease With Creatinine, Cystatin C, and Urine Albumin-to-Creatinine Ratio and Association With Progression to End-Stage Renal Disease and Mortality," *JAMA*, vol. 305, no. 15, p. 1545, Apr. 2011, doi: 10.1001/jama.2011.468.

[53] L. A. Stevens, S. Padala, and A. S. Levey, "Advances in glomerular filtration rate-estimating equations," *Curr Opin Nephrol Hypertens*, vol. 19, no. 3, pp. 298–307, May 2010, doi: 10.1097/MNH.0b013e32833893e2.

[54] S. A. Shaikh, "Measures Derived from a 2 x 2 Table for an Accuracy of a Diagnostic Test," *J Biom Biostat*, vol. 02, no. 05, 2011, doi: 10.4172/2155-6180.1000128.

[55] H. J. Kim, D. Park, Y. Park, D. H. Kim, and J. Kim, "Electric-Field-Mediated In-Sensor Alignment of Antibody's Orientation to Enhance the Antibody-Antigen Binding for Ultrahigh Sensitivity Sensors," *Nano Lett*, vol. 22, no. 16, pp. 6537–

6544, Aug. 2022, doi: 10.1021/ACS.NANOLETT.2C01584/SUPPL_FILE/NL2C01584_SI_001.PDF.

[56] J. M. Bland and D. G. Altman, “Measuring agreement in method comparison studies,” *Stat Methods Med Res*, vol. 8, no. 2, pp. 135–160, Jun. 1999, doi: 10.1191/096228099673819272.

[57] S. W. Benoit, E. A. Ciccia, and P. Devarajan, “Cystatin C as a biomarker of chronic kidney disease: latest developments,” *Expert Rev Mol Diagn*, vol. 20, no. 10, pp. 1019–1026, Oct. 2020, doi: 10.1080/14737159.2020.1768849.

[58] A.-S. Bargnoux *et al.*, “Multicenter Evaluation of Cystatin C Measurement after Assay Standardization,” *Clin Chem*, vol. 63, no. 4, pp. 833–841, Apr. 2017, doi: 10.1373/clinchem.2016.264325.

[59] J. H. Eckfeldt, A. B. Karger, W. G. Miller, G. P. Rynders, and L. A. Inker, “Performance in Measurement of Serum Cystatin C by Laboratories Participating in the College of American Pathologists 2014 CYS Survey,” *Arch Pathol Lab Med*, vol. 139, no. 7, pp. 888–893, Jul. 2015, doi: 10.5858/arpa.2014-0427-CP.

[60] S. Natarajan, M. C. Derosa, M. I. Shah, and J. Jayaraj, “Development and evaluation of a quantitative fluorescent lateral flow immunoassay for cystatin-c, a renal dysfunction biomarker,” *Sensors*, vol. 21, no. 9, p. 3178, May 2021, doi: 10.3390/S21093178/S1.

[61] S. K. Bikkarolla, K. Venkatesan, Y. R. Revathy, S. Parameswaran, S. Krishnakumar, and D. Dendukuri, “The Quantitative Detection of Cystatin-C in Patient Samples Using a Colorimetric Lateral Flow Immunoassay,” *Biosensors (Basel)*, vol. 14, no. 1, Jan. 2024, doi: 10.3390/bios14010030.

[62] Y.-C. Ma *et al.*, “Improved GFR estimation by combined creatinine and cystatin C measurements,” *Kidney Int*, vol. 72, no. 12, pp. 1535–1542, Dec. 2007, doi: 10.1038/sj.ki.5002566.

[63] C. White *et al.*, “Estimating Glomerular Filtration Rate in Kidney Transplantation,” *Journal of the American Society of Nephrology*, vol. 16, no. 12, pp. 3763–3770, Dec. 2005, doi: 10.1681/ASN.2005050512.

[64] H. Sato *et al.*, “Cystatin C is a sensitive marker for detecting a reduced glomerular filtration rate when assessing chronic kidney disease in patients with rheumatoid arthritis and secondary amyloidosis,” *Scand J Rheumatol*, vol. 39, no. 1, pp. 33–37, Jan. 2010, doi: 10.3109/03009740903042402.

[65] U. Pöge, T. Gerhardt, B. Stoffel-Wagner, H. U. Klehr, T. Sauerbruch, and R. P. Woitas, “Calculation of glomerular filtration rate based on Cystatin C in cirrhotic patients,” *Nephrology Dialysis Transplantation*, vol. 21, no. 3, pp. 660–664, Mar. 2006, doi: 10.1093/ndt/gfi305.

[66] Y. Bouvet *et al.*, “GFR is better estimated by considering both serum cystatin C and creatinine levels,” *Pediatric Nephrology*, vol. 21, no. 9, pp. 1299–1306, Sep. 2006, doi: 10.1007/s00467-006-0145-z.

[67] L. A. Stevens *et al.*, “Estimating GFR Using Serum Cystatin C Alone and in Combination With Serum Creatinine: A Pooled Analysis of 3,418 Individuals With CKD,” *American Journal of Kidney Diseases*, vol. 51, no. 3, pp. 395–406, Mar. 2008, doi: 10.1053/j.ajkd.2007.11.018.

[68] D. C. Chen, O. A. Potok, D. Rifkin, and M. M. Estrella, “Advantages, Limitations, and Clinical Considerations in Using Cystatin C to Estimate GFR.,” *Kidney360*, vol. 3, no. 10, pp. 1807–1814, Oct. 2022, doi: 10.34067/KID.0003202022.

[69] A. B. Karger, T. Long, L. A. Inker, and J. H. Eckfeldt, “Improved Performance in Measurement of Serum Cystatin C by Laboratories Participating in the College of American Pathologists 2019 CYS Survey,” *Arch Pathol Lab Med*, vol. 146, no. 10, pp. 1218–1223, Oct. 2022, doi: 10.5858/arpa.2021-0306-CP.

[70] M. Dong *et al.*, “Rapid and Low-Cost CRP Measurement by Integrating a Paper-Based Microfluidic Immunoassay with Smartphone (CRP-Chip),” *Sensors 2017, Vol. 17, Page 684*, vol. 17, no. 4, p. 684, Mar. 2017, doi: 10.3390/S17040684.

[71] S. Natarajan, M. Derosa, J. Joseph, M. I. Shah, and S. Karthik, “Aptamer based lateral flow assays for rapid and sensitive detection of CKD marker Cystatin C,” in *2021 IEEE International Symposium on Medical Measurements and Applications, MeMeA 2021 - Conference Proceedings*, Institute of Electrical and Electronics Engineers Inc., Jun. 2021. doi: 10.1109/MeMeA52024.2021.9478684.

[72] “i-STAT 1 | Abbott Point of Care.” Accessed: May 06, 2025. [Online]. Available: https://www.globalpointofcare.abbott/us/en/product-details/apoc/i-stat-system-us.html

[73] “U-Scan | Withings.” Accessed: Apr. 23, 2025. [Online]. Available: https://www.withings.com/ca/en/u-scan?srsltid=AfmBOooihIwVXkge-6jJkHMMT4idL4ylNibi7QXgtQQK7M20gFmi66xa

[74] “DCA Vantage® Analyzer - Siemens Healthineers Canada.” Accessed: Apr. 23, 2025. [Online]. Available: https://www.siemens-healthineers.com/en-ca/diabetes/analyzers/dca-vantage-analyzer

[75] R. Hiraoka *et al.*, “Paper-Based Device for Naked Eye Urinary Albumin/Creatinine Ratio Evaluation,” *ACS Sens*, vol. 5, no. 4, pp. 1110–1118, Apr. 2020, doi: 10.1021/ACSSENSORS.0C00050/SUPPL_FILE/SE0C00050_SI_001.PDF.

[76] C. D. Chin *et al.*, “Microfluidics-based diagnostics of infectious diseases in the developing world,” *Nature Medicine 2011 17:8*, vol. 17, no. 8, pp. 1015–1019, Jul. 2011, doi: 10.1038/nm.2408.